Electrical resistivity at large temperatures: Saturation and lack thereof

M. Calandra and O. Gunnarsson

Max-Planck-Institut für Festkörperforschung D-70506 Stuttgart, Germany

Many transition metal compounds show a saturation of the electrical resistivity at high temperatures T while the alkali-doped fullerenes and the high-T_c cuprates are usually considered to show no saturation. We present a model of transition metal compounds, which shows saturation, and a model of alkali-doped fullerenes, which shows no saturation. The electron scattering is assumed to be due to interaction with phonons. The properties of these models are determined by performing quantum Monte Carlo calculations. To analyze the results, as well as earlier results for the high-T_c cuprates, we use the f-sum rule. We demonstrate that the f-sum rule leads to a natural upper limit for the resistivity, which usually has a weak T dependence. For some systems and at low T, the resistivity increases so rapidly that this upper limit is approached for experimentally accessible temperatures. The resistivity then saturates. For a model of transition metal compounds with weakly interacting electrons, the upper limit corresponds to an apparent mean free path consistent with the Ioffe-Regel condition. For a model of the high-T_c cuprates with strongly interacting electrons, however, the upper limit is much larger than the Ioffe-Regel condition suggests. This upper limit is not exceeded by experimental resistivities. The experimental data for the cuprates are therefore consistent with saturation. After saturation the resistivity normally grows slowly. The alkali-doped fullerenes can be considered as systems where saturation has happened already for $T=0$, due to orientational disorder. We show, however, that for these systems the resistivity grows so rapidly after ''saturation'' that this concept is meaningless. This is due both to the small band width and to the coupling to the level energies of the important (intramolecular) phonons in the fullerenes.

I. INTRODUCTION

The electrical resistivity of metals is often described in a semiclassical picture, where an electron on the average travels a mean free path l before it is scattered by a phonon, an impurity or another electron. Assuming a spherical Fermi surface, the resistivity ρ can be expressed in terms of l as

$$\rho = \frac{3\pi^2\hbar}{e^2 k_F^2 l}, \tag{1}$$

where k_F is the Fermi wave vector. Alternatively, if we know the resistivity experimentally, we can deduce an apparent mean free path from Eq. (1). For a good metal, l is typically several hundred Å or more. As the temperature T is increased, ρ increases. Normally, it is found that $\rho(T) \sim T$ for T larger than some fraction of a typical phonon energy. This is due to the increased scattering by phonons, and it corresponds to a reduction of l. Nevertheless, at the melting point, l is still typically very much larger than the separation d of two neighboring atoms. An example of this behavior is given by Cu in Fig. 1.

In the 1970's a number of exceptions to this behavior were found.[1] In particular for several $A15$ compounds, such as Nb_3Sb and Nb_3Sn, it was found that ρ increases very rapidly with T for small T, leading to very large values already for temperatures of the order of a few hundred K. At these values of T, the slope of $\rho(T)$ is strongly reduced. This is shown in Fig. 1, where the resistivities of Nb_3Sb and Cu are compared. This was described as ''resistivity saturation.''[1] Interestingly, it was found that saturation happened when $l \sim d$, the Ioffe-Regel condition.[2] The corresponding resistivity is also shown in Fig. 1. During the

1970's and early 1980's many examples of this were studied, and saturation of the resistivity when $l \sim d$ was considered a universal behavior.[3]

In a semiclassical picture, this behavior may be expected. It may seem that the worst that could happen is that an electron is scattered at every atom. We would then expect $l \sim d$ to be fulfilled. This argument is, however, not convincing. In the semiclassical theory, it is assumed that an electron travels through the solid with a well-defined **k** vector between the scattering events. If, however, $l \sim d$, it is not possible to define **k**, and the theory breaks down.[4] A proper theory of saturation is therefore needed. A number of theories have been put forward,[5–7] but no theory has been generally ac-
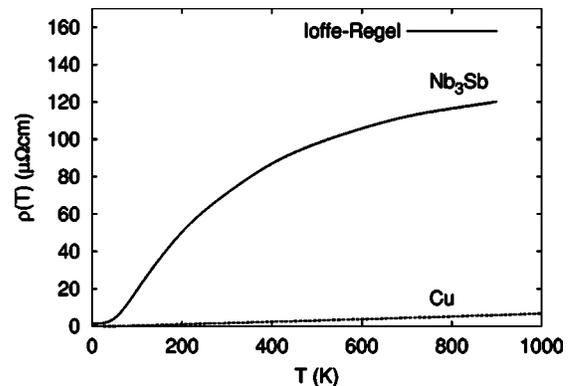

FIG. 1. Resistivities of Cu and Nb_3Sb (Ref. 1). The figure also shows the Ioffe-Regel (Ref. 2) saturation resistivity for Nb_3Sb, obtained by assuming that the mean free path l in Eq. (1) is equal to the the distance between the neighboring atoms. The figure illustrates that for Nb_3Sb the resistivity saturates at roughly the value expected from the Ioffe-Regel criterion (Ref. 2).
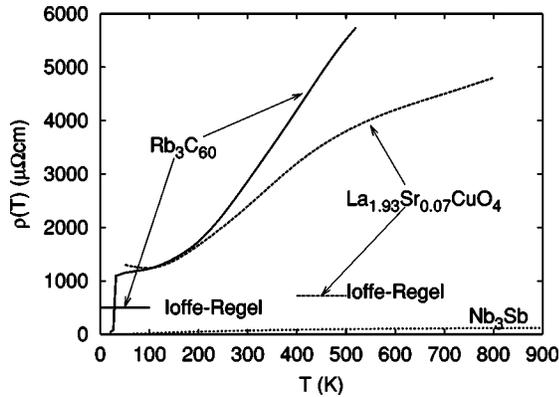
FIG. 2. Resistivities of $La_{1.93}Sr_{0.07}CuO_4$ (Ref. 8) and Rb_3C_{60} (Ref. 9) and the corresponding Ioffe-Regel (Ref. 2) saturation resistivities (Ref. 11). The figure illustrates that the resistivity of these systems becomes much larger than predicted by the Ioffe-Regel condition.

cepted. Due to the break down of the semiclassical theory when $l \sim d$, the concept of a mean free path itself becomes questionable for such small values of l. In this case we use Eq. (1) as a definition of the (apparent) mean free path.

More recently, several apparent exceptions to resistivity saturation have been found. In particular, this is the case for some strongly correlated systems, for instance the high-T_c cuprates,[8] and for the alkali-doped fullerenes.[9,10] This is illustrated in Fig. 2, where we show the resistivities of $La_{1.93}Sr_{0.07}CuO_4$ and Rb_3C_{60} together with the Ioffe-Regel resistivities.[11] Different experiments for alkali-doped C_{60} compounds show substantial differences, but this is not essential for the present discussion. The Ioffe-Regel resistivities of these two systems are very large, due to the low carrier density. The figure illustrates that the experimental resistivities, nevertheless, greatly exceed the Ioffe-Regel resistivities. It also illustrates that the resistivities of these two compounds are very much larger than for Nb_3Sb and other systems, which shows saturation according to the Ioffe-Regel condition.

This shows that the semiclassical argument behind the Ioffe-Regel condition is not only questionable, but that it leads to wrong conclusions for the high-T_c cuprates and the C_{60} compounds. This emphasizes the need for a proper theory of why saturation happens for some systems but not for others. We also need to understand why saturation happens for most transition metal compounds when $l \sim d$, although l is not a well-defined concept any more.

We have earlier presented such a theory for transition metal compounds in a short publication,[12] and we here expand the arguments. We have also analyzed the reasons for the lack of saturation in the alkali-doped C_{60} compounds,[13] and we provide additional results here. Finally, we have presented results for a model of the high-T_c cuprates.[14] We have therefore considered models of three classes of systems: (i) a model of weakly correlated transition metal compounds, which shows saturation in agreement with the Ioffe-Regel condition, (ii) a model of strongly correlated high-T_c compounds, which shows saturation but at much larger values

than predicted by the Ioffe-Regel conditions, and (iii) a model of alkali-doped fullerenes, which shows no saturation.

We assume that in cases (i) and (iii) the important scattering is due to the electron-phonon interaction. In a model Hamiltonian approach, there are two natural types of coupling to the phonons, either via the level energies (LE's) coupling or via the hopping matrix integrals (HI's) coupling. In most nonionic compounds the latter effect should be the dominating one. As the distance between two neighboring atoms is changed due to the excitation of a phonon, the main effect should be a change of the hopping integrals. We study this for a model of transition metal compounds, referred to as the TM model.

In molecular solids, such as the alkali-doped fullerenes, the situation is different. Due to the weak coupling between the molecules, it is sensible to first calculate the levels of a free molecule, and then to study the weak hopping between these levels. In the alkali-doped fullerenes the main coupling is to intramolecular phonons. These phonons couple primarily to the level energies and only weakly to the hopping integrals between the molecules. We therefore study the LE coupling for a model of alkali-doped C_{60} systems, in the following referred to as the C_{60} model. The LE coupling may also become important for strongly ionic systems.

We use a quantum Monte Carlo (QMC) method[15] for calculating the current-current correlation function for imaginary times. A maximum entropy method[16] is then applied to analytically continue the response function to the real frequency axis. This gives the frequency dependent optical conductivity $\sigma(\omega)$ and the resistivity $\rho = 1/\sigma(\omega = 0)$. Since the QMC method has no sign problem for the models studied here, we are able to obtain rather accurate results for the resistivity. In particular, we can establish whether or not the models we consider show resistivity saturation.

To interpret the results we use a simplified approximate approach, treating the phonons (semi)classically. In this method we assume that the phonons can be described by random static displacements of the atoms with an average amplitude that increases with T. The remaining electronic problem can then easily be solved quantum mechanically. This approach is in contrast to the Boltzmann equation, where the electrons are treated semiclassically. The main advantage of this method, compared with the QMC calculation, is that it is simple enough to allow an interpretation of the results. By comparing with the QMC results we establish the range of applicability of the semiclassical method for the models of interest here.

In our semiclassical treatment, the excitation of phonons leads to a static variation of the level energies in the C_{60} model and of the hopping integrals in the TM model. In the context of disordered systems, this is referred to as diagonal and off-diagonal disorder, respectively. Past work has primarily studied diagonal disorder, which in some respects is technically simpler.

Traditionally, transport is described within the Boltzmann theory. The Bloch-Boltzmann[17] theory starts from the perfectly periodic system, and treats the scattering mechanisms as small perturbations. This can be considered as a theory which is valid to lowest order in $1/(k_F l)$.[4] This further em-

pahsizes that the Boltzmann equation becomes questionable when $l \sim d$. Furthermore, the Ziman approximation[18] to the Boltzmann equation leads to $\rho(T) \sim T$ for large T, i.e., there is no saturation in contrast to what is found experimentally for many systems. It is then natural to look for extensions of the Boltzmann equations, which would extend the range of perturbation strengths that can be treated.[5,6] We find, however, that in, e.g., the $A15$ compounds the thermally excited phonons even at relatively small T tend to largely remove the effects of periodicity. In the semiclassical treatment of the phonons, the momentum conservation in the electronic system is lost already for temperatures of the order of a few hundred K. We therefore consider the opposite limit to the Boltzmann equation, where we assume that thermal excitations have completely destroyed periodicity. At low T there is a Drude peak in the optical conductivity $\sigma(\omega)$ due to intraband transitions between states with similar **k** vectors. As T is increased, **k** conservation is lost, the meaning of intraband transitions is blurred, and the Drude peak disappears. We therefore focus on the limit where there is no pronounced structure in $\sigma(\omega)$ at small ω.

We have earlier used current and charge conservation to obtain simple upper estimates for the resistivity of a metal.[12] Here we show how the same result can be derived by using the (related) f-sum rule. This approach has the advantage that it can also be used to discuss the high-T_c cuprates,[14] and that it is convenient for discussing the fullerenes. The approach based on the f-sum rule therefore provides the most convenient framework for analyzing the different classes of materials.

We combine the f-sum rule with the assumption that the Drude peak is lost. This naturally leads to an upper limit for the resistivity, which usually has a weak T dependence. If the initial slope of $\rho(T)$ is very large, $\rho(T)$ reaches this limiting value already for experimentally available values of T. At this point saturation normally happens, as is illustrated in our TM model. The removal of the Drude peak could be due to any scattering mechanism, e.g., electron-phonon (HI or LE coupling), electron-electron, or disorder scattering. For the TM model considered here, we show in a quantum mechanical treatment that saturation should happen roughly when the Ioffe-Regel criterion is satisfied. This is somewhat accidental and it is not true for a model of the high-T_c cuprates, where strong correlation effects leads to a larger saturation resistivity.

While a pronounced saturation is observed for the $A15$ compounds Nb_3Sb or Nb_3Sn, other systems, such as Nb, show a weaker saturation or no saturation at all. Here we study a simple model of $A15$ compounds, referred to as the Nb_3^* model,[19] where we include the d orbitals of the Nb atoms, put on the appropriate $A15$ lattice, but where the remaining atom (e.g., Sn in Nb_3Sn) is neglected. This is compared with Nb, where the atoms are put on a bcc lattice. These two models then only differ with respect to the lattice structure. This difference leads to a smaller plasma frequency for Nb_3Sb and a steeper slope of $\rho(T)$. This leads to a much more pronounced saturation for Nb_3Sb.

Even after "saturation" has happened, $\rho(T)$ tends to continue to grow, but at a slower rate. In this respect there is

sometimes an essential distinction between LE and HI coupling. This can be best discussed using the f-sum rule. We show that the upper limit of the resistivity is obtained from the ratio of the band width and the kinetic energy. These two quantities keep growing without limit with T, due to the Bose nature of the phonons and the lack of limitation on the number of phonons. The changes of these two quantities work together for the LE coupling, but tend to compensate each other for the HI coupling. As a result the resistivity grows more slowly after "saturation" for the HI coupling and the saturation is more pronounced. This distinction is fairly clear cut for the C_{60} model. For this model, disorder leads to such a strong scattering, that "saturation" can be considered to have happened already at $T=0$. Due to the LE coupling and the small band width, however, $\rho(T)$ grows so rapidly after "saturation" that the concept of saturation becomes meaningless. For HI coupling, on the other hand, the resistivity shows a clear change in slope, even for the C_{60} model.

In Sec. II we present the TM and C_{60} models and in Sec. III the QMC and semiclassical methods are described. The results are presented in Sec. IV and discussed in Sec. V. In Sec. VI we summarize the present results as well as earlier results for the high-T_c cuprates in the framework of the f-sum rule.

II. MODELS

A. TM model

We first consider a model appropriate for a transition metal (compound), referred to as the TM model. Each transition metal atom has a fivefold degenerate ($n=5$) level. It couples to the other atoms via hopping matrix elements $t_{\mu\nu}$, where $\nu \equiv (m,i)$ is a combined label for a orbital index m and a site index i. Thus the electronic Hamiltonian is

$$H^{\text{el}} = \varepsilon_0 \sum_{\mu\sigma} c_{\mu\sigma}^{\dagger} c_{\mu\sigma} + \sum_{\mu\nu\sigma} t_{\mu\nu} c_{\mu\sigma}^{\dagger} c_{\nu\sigma}, \qquad (2)$$

where $c_{\mu}^{\dagger}$ creates an electron in the state $|\mu\rangle$. As discussed in the Introduction, we consider two different models where the atoms are put on a bcc or an $A15$ lattice, describing a transition metal (Nb) or an $A15$ compound, respectively. As discussed above, in the case of the $A15$ compound we only consider the transition metal atoms and, for instance, neglect Sb in Nb_3Sb.[19] This is referred to as the Nb_3^* model.

To describe the hopping integrals, we essentially follow Harrison,[20] and assume that the radial part of the integrals has a power dependence on the separation of the atoms. However, instead of the power five, used by Harrison, we use the power 3.6, more appropriate for Nb.[21] Using Harrison notation for the radial part between two atomic d energy levels

$$V_{dd,s} = \eta_{dd,s} \frac{\hbar^2 r_d^{1.6}}{m} \frac{1}{|\mathbf{R}_i - \mathbf{R}_j|^{3.6} + a_0^{3.6}} \qquad (3)$$

where $\eta_{dd,\sigma} = -16.2, \eta_{dd,\pi} = 8.75$, and $\eta_{dd,\delta} = 0$ and m is the electron mass. The parameter r_d has been chosen in order to reproduce the band with as obtained from LDA calcula-

tions for Nb_3^*,[19] namely, $r_d = 0.7$. Since the atoms vibrate, their separation can occasionally become very small. To avoid that the hopping integrals then become very large, we have introduced the term containing a_0 in the denominator. We use $a_0 = 2$ Å. Equation (3) shows the distance dependence. In addition there are angular factors, depending on which m-quantum numbers are involved, as described by Harrison.[20] In the model of Nb we only consider nearest neighbor hopping, while in the $A15$ model (Nb_3^*) also second nearest neighbor hopping is included, since the second nearest neighbors are not much further away then the nearest neighbors.

We consider the case when the phonons couple to the hopping integrals (HI's). The phonons are approximated as Einstein phonons. The frequency $\omega_{ph} = 0.014$ eV was obtained from the average frequency of Nb metal.[22] For each Nb atom we introduce one such phonon in each coordinate direction. The x coordinate of atom i is then given by

$$R_{ix} = R_{ix}^0 + \sqrt{\frac{\hbar}{2M\omega_{ph}}}(b_{ix} + b_{ix}^\dagger), \tag{4}$$

where R_{ix}^0 is the unperturbed x coordinate of the atom i, $b_{ix}^\dagger$ creates a phonon in the x direction on site i, and M is the mass of a Nb atom. These vibrations couple to the hopping matrix elements.

To obtain the conductivity we calculate the current-current correlation function. This requires a definition of the matrix elements of the current operator. In our model Hamiltonian approach, it is not appropriate to calculate these as expectation values of the current operator between some basis functions, since the basis functions underlying our model Hamiltonian are not explicitly defined. Instead one can use charge and current conservation, i.e., the requirement that the change of density inside some small volume is equal to the current entering this volume. This leads to the result

$$\hat{\mathbf{j}}_{\mu\nu} = \frac{ie}{\hbar}(\mathbf{R}_i - \mathbf{R}_j)t_{\mu\nu}, \tag{5}$$

where $\mu \equiv (m,i)$ and $\nu \equiv (m',j)$.

B. C_{60} model

We next consider a model appropriate for alkali-doped fullerenes, referred to as the C_{60} model. In these systems the t_{1u} band is partly occupied, and we therefore consider a model with a threefold degenerate t_{1u} orbital on each C_{60} molecule i. These orbitals are connected by nearest neighbor hopping matrix elements. For the electronic part we therefore use the same form of the Hamiltonian as above [Eq. (2)], but the orbitals are now threefold degenerate and placed on a fcc lattice.

The hopping integrals are obtained from a tight-binding description.[23,24] For each of the 60 C atoms in a C_{60} molecule we introduce one $2p$ orbital pointing radially out from the molecule. We then generate orbitals of t_{1u} character by forming linear combinations of the 60 $2p$ orbitals. The hopping between the t_{1u} orbitals on different molecules is then deter-

mined by the hopping between $2p$ orbitals on different molecules. The $2p$ orbitals couple via σ and π hopping integrals. We use

$$V_\sigma = V_0 d e^{-(d-d_0)/L}, \tag{6}$$

$$V_\pi = -V_\sigma/4, \tag{7}$$

where $V_0 = 9.85$ eV, $d_0 = 1.43$ Å, and $L = 0.505$ Å. The calculations were performed for the lattice parameter 14.24 Å. In most calculations we take into account[23,25] the orientational disorder[26] of the C_{60} molecules.

The important electron-phonon coupling is due to the intramolecular phonons of H_g symmetry. There are eight such phonons in C_{60}, each one being a five-fold degenerate Jahn-Teller mode. Here we only include one degenerate H_g mode per site. We use the Hamiltonian

$$H^{\text{el-ph}} = \frac{g}{2}\sqrt{\frac{2M\omega_{ph}}{\hbar}}\sum_{\gamma=1}^{5}\sum_{i\sigma}\sum_{m=1}^{3}\sum_{m'=1}^{3}V_{mm'}^{(\gamma)}\psi_{im\sigma}^\dagger\psi_{im'\sigma}x_{i\gamma}, \tag{8}$$

where $x_{i\gamma}$ is the phonon coordinate for a phonon with quantum number γ on site i, g is an overall coupling strength, and $V_{mm'}^{(\gamma)}$ are dimensionless coupling constants[27,28] given by symmetry. The dimensionless electron-phonon coupling constant is given by

$$\lambda = 5\frac{g^2}{\omega_{ph}}N(\mu), \tag{9}$$

where $N(\mu)$ is the density of states per spin, orbital, and molecule at the Fermi energy. The current matrix elements are given by Eq. (5) with $\mathbf{R}_i = \mathbf{R}_i^0$.

As a comparison, we also consider a C_{60} model where the intermolecular phonons couple to the hopping integrals (HI coupling), instead of the LE coupling considered above. This coupling is obtained by displacing the molecules from their ideal positions of the fcc lattice due to the excitations of intermolecular phonons. For large values of T, the molecules come unrealistically close to each others in our semiclassical theory, neglecting the strongly repulsive interaction for small separations, and the hopping integrals become unrealistically large. For this reason we introduce a modification of the hopping integrals between the $2p$ orbitals in the case of the HI coupling . The exponent $e^{-(d-d_0)/L}$ is replaced by

$$e^{-(d_1-d_0)/L}\frac{e^{(d_1-d_0)/L} + e^{(d_2-d_0)/L}}{e^{(d-d_0)/L} + e^{(d_2-d_0)/L}}, \tag{10}$$

where $d_1 = 3.1$ Å is the separation of the nearest C atoms on neighboring molecules in the equilibrium position and $d_2 = 2$ Å. For $d \gg d_2$, the hopping integrals are essentially unchanged, and for $d = d_1$ they are exactly unchanged, while for $d \ll d_2$ the hopping integral is cut off at a value which is factor 10 larger than in equilibrium.

III. METHODS

A. Quantum Monte Carlo method

To establish the properties of our models, we use a quantum Monte Carlo (QMC) approach.[15] For these models, the QMC method has no so-called sign problem, thanks to the absence of a repulsive Coulomb interaction. In the calculation of response functions for imaginary times there are then only statistical errors which can be made arbitrarily small by improving the sampling. These response functions are analytically continued to the real frequency axis by using a maximum entropy method.[16] Although it is nontrivial to control the errors in this method, it should still be quite accurate for the response functions considered here, due to the simple form of their spectra. Thus we are able to quite accurately establish the large T behavior of the resistivity for models with coupling to phonons.

In the QMC approach used here,[15] the starting point is the partition function

$$Z = \text{Tr}\, e^{-H/T}, \qquad (11)$$

where Tr is a trace over all states. An imaginary time τ is introduced, $0 \leq \tau \leq \beta = 1/(k_B T)$. The partition function can then be expressed as a functional integral over the phonon coordinates as a function of τ. For given values of the phonon coordinates, the electronic part of the Hamiltonian is a one-particle Hamiltonian. The electronic degrees of freedom can then be integrated out and be expressed as a determinant. Finally, the phonon coordinates are sampled in a Monte Carlo approach.

For the LE coupling, the phonons are local and only influence the levels on the molecule of the phonon. For the C_{60} model, this corresponds to a 3×3 block in the determinant obtained in the approach above. The change of the determinant when one phonon coordinate is changed can then easily be obtained in an updating approach.[15] For the HI coupling, on the other hand, each phonon influences the hopping integrals to the neighbors of the atom of the phonon. Different phonons then couple to partly "overlapping" blocks. It is then not possible to introduce the simple block form used in the C_{60} model. This leads to a substantially more complicated updating approach, which is discussed in Appendix A.

B. Semiclassical method

While the QMC method above is very useful in establishing the properties of our models, its complexity means that it is hard to interpret the results. We therefore introduce a much simpler method, where the phonons are treated semiclassically. We demonstrate that this method is quite accurate for the TM model with HI coupling, by showing that it agrees quite well with the accurate QMC calculations. For the C_{60} model with LE coupling, the accuracy is less good, in particular for large T. The method is, nevertheless, useful for the interpretation.

We consider a large supercell with L unit cells, K atoms per unit cell and a total of $N = KL$ atoms. Periodic boundary
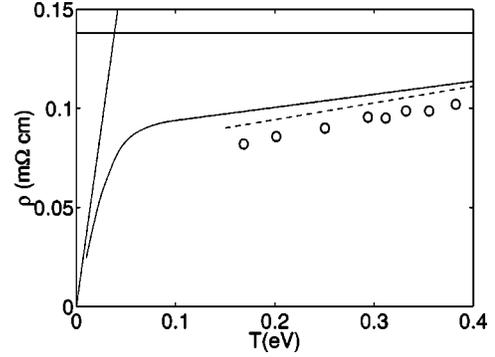

FIG. 3. Resistivity $\rho(T)$ as a function of temperature T for Nb_3^*. The figure compares the semiclassical [broken ($N=36$) and full ($N=648$) curves] and QMC (circles, $N=36$) calculations. The figure also shows the small [Eq. (25)] and large [Eq. (21)] temperature results. The figure illustrates that the resistivity of the TM model saturates at large T. Comparison with the QMC results, shows that the semiclassical calculation is quite accurate, at least for large T.

conditions are used. Each phonon coordinate is given a random displacement according to a Gaussian distribution centered at zero and the width

$$\langle x^2 \rangle = \frac{\hbar}{M \omega_{\text{ph}}} n_B(T), \qquad (12)$$

where

$$n_B(T) = \frac{1}{e^{\hbar \omega_{\text{ph}}/(k_B T)} - 1}, \qquad (13)$$

is the occupation of the phonon mode. In this way, a set of displaced coordinates are obtained. These define a one-particle Hamiltonian for the electrons. In the case of HI coupling, we simply calculate the hopping matrix elements using the displaced atomic positions. For the LE coupling, we insert the phonon displacements in Eq. (8). Since the coupling contains a factor $\sqrt{M}$, the Hamiltonian is independent of M for a given λ and ω_{ph} in the case of the LE coupling.

To calculate optical conductivity, we find the eigenstates $|l\rangle$ and eigenvalues ε_l of this Hamiltonian. The optical conductivity is then given by

$$\sigma(\omega) = \frac{2\pi}{N\Omega\omega} \sum_{ll'} |\langle l|\hat{j}_x|l'\rangle|^2 (f_l - f_{l'}) \delta(\hbar\omega - \varepsilon_{l'} + \varepsilon_l), \qquad (14)$$

where Ω is the volume per atom and f_l is the Fermi function for the energy ε_l. The prefactor 2 comes from the summation over spin. We have assumed that the system is isotropic, so that it is no limitation to consider the conductivity in the x direction.

Figure 3 compares the QMC (circles) and semiclassical (broken curve) methods for Nb_3^* with $N=36$ atoms in the supercell. The QMC calculation has been limited to rather large values of T, which is the range of particular interest here, and which is also the range of T where the calculation can be performed with a reasonable numerical effort. The
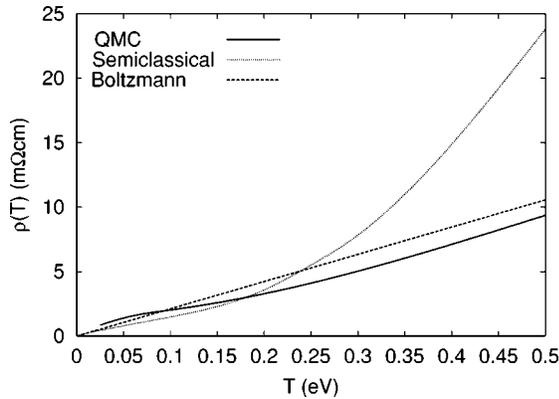
FIG. 4. Resistivity $\rho(T)$ as a function of temperature T in the ordered C_{60} model for $\omega_{ph} = 0.00001$ eV and $\lambda = 0.6$. The figure compares the QMC (full curve), the semiclassical (dotted curve), and the Boltzmann (broken curve) results. The phonon frequency was chosen to be so small that $\rho(T) \sim T$ in the Boltzmann theory for all T of interest.
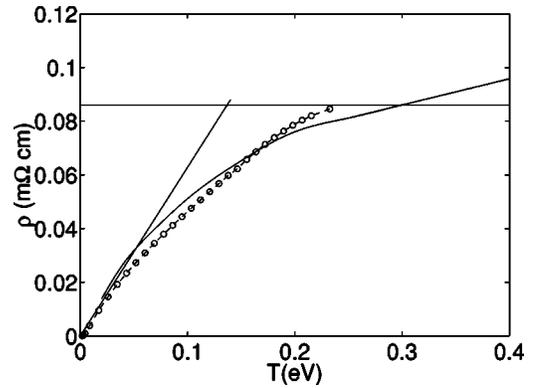

FIG. 5. Resistivity $\rho(T)$ as a function of temperature T for Nb according to a semiclassical calculation. The figure compares the semiclassical (full curve) calculation for $N = 640$ with experimental results (circles) (Ref. 29). It shows the small [Eq. (25)] and large [Eq. (21)] temperature results. The figure illustrates that there is saturation also for Nb at large T in good agreement with experiment.

figure illustrates that the semiclassical calculation is quite accurate at large T for the TM model. By comparing the semiclassical calculation for $N = 36$ and $N = 648$ we also illustrate that at large T the result does not change much if the size of the supercell is increased. For small values of T, however, the discreteness of the levels for $N = 36$ would prevent a reliable semiclassical calculation for this super cell size.

Figure 4 compares the semiclassical theory (dotted curve) with the QMC (full curve) and the Boltzmann (broken curve) theories for the C_{60} model with LE coupling, assuming ordered C_{60} molecules. The small-T behavior is discussed in detail in Sec. V F. Here we just notice that the semiclassical theory agrees with the Boltzmann theory for very small T and that it agrees approximately with the QMC results for small and intermediate values of T. There is, however, a qualitative disagreement for large T. The reason is that the strong static diagonal disorder introduced by the phonons in the semiclassical theory for large T leads to localization. This is discussed in more detail in Sec. V H. While the semiclassical theory for the C_{60} model with LE coupling is sufficiently accurate to analyze the results for small and intermediate values of T, it is less accurate than for the TM model with HI coupling, in particular for large T. This is further discussed in Sec. V H.

IV. RESULTS

A. TM model

The full curve in Fig. 3 shows the semiclassical results for the Nb_3^* model. It illustrates how the resistivity shows a very pronounced saturation already at quite small temperatures. The calculated resistivity at large T agrees rather well with the experimentally results, e.g., about 0.12 mΩ cm at $T = 900$ K (0.08 eV).[1] This agreement with experiment is important, since, as we discuss below, our saturation resistivity [Eq. (21)] essentially only depends on the nearest-neighbor distance, the orbital degeneracy n, the filling and the lattice

structure. This illustrates that our TM model is appropriate for describing resistivity saturation. For small T, the resistivity grows slower than what is found experimentally, which is probably due to the electron-phonon interaction being somewhat underestimated in our simple model.

Figure 5 compares the semiclassical results for Nb with experimental results. The figure shows a surprisingly good agreement between theory and experiment, given the simplicity of the model and the absence of adjustable parameters. The figure illustrates that saturation also happens for Nb, but at a much larger temperature scale than for Nb_3^*. The reason for this difference is discussed in Sec. V D.

B. C_{60} model

Figure 6 shows QMC calculations for the resistivity of the C_{60} model. It illustrates that there is no sign of saturation. Actually the curves tend to bend slightly upwards for large T. The x indicates the resistivity due to the orientational disorder. This $T = 0$ resistivity was calculated from Eq. (14), i.e., independently of the QMC formalism. The curve for $\lambda = 0.80$ shows signs of superconductivity at small T, since the curve turns sharply downwards as T is lowered, due to superconducting fluctuations. For a still larger value of λ the system behaves as an insulator, as illustrated by the negative slope of $\rho(T)$ for small T.

The solid curve show the result for $\lambda = 0$. In this case the resistivity is entirely due to the orientational disorder of the C_{60} molecules. It is interesting that this ''T-independent'' scattering mechanism gives rise to a weak T dependence. The reason for this are discussed in Sec. V E.

The results for Rb_3C_{60} in Fig. 2 were measured at a constant pressure and show an approximately quadratic dependence on T. If these results are converted to a constant volume measurement, however, an approximately linear dependence on T is found down to $T \sim 100-200$ K. In agreement with this, Fig. 6, $\rho(T)$ shows a rather linear de-
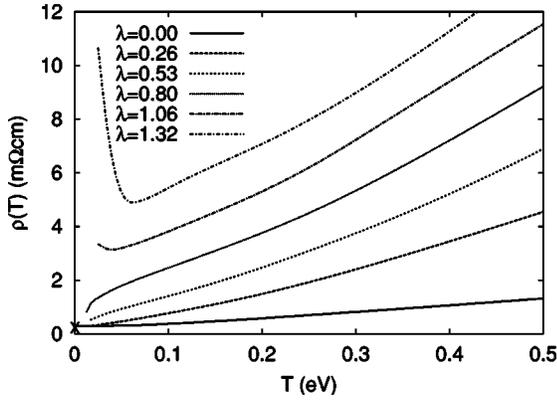
FIG. 6. Resistivity $\rho(T)$ as a function of temperature T and electron-phonon coupling λ for the C_{60} model according to QMC calculations. The phonon frequency is $\omega_{ph} = 0.1$ eV. The figure illustrates the lack of saturation. For $\lambda = 0.80$ the onset of superconductivity can be seen as a sharp downturn in $\rho(T)$ as T is lowered, due to superconducting fluctuations. For $\lambda = 1.06$ and 1.32, the resistivity has a negative slope for small T, indicating an insulating system. The x shows the resistivity due to orientational disorder.

pendence for $\lambda \lesssim 0.8$ until the superconductivity fluctuations set in. The reason for this behavior have been discussed earlier.[13]

C. Comparison of HI and LE coupling

The results for the TM and C_{60} models differ drastically. While the TM model shows saturation, the C_{60} model does not. It is interesting to ask to what extent this is due to a difference in the electron-phonon coupling (HI versus LE coupling) and to what extent it is due to other differences, such as the size of the unit cell, the lattice structure and the band width. For this reason we have also studied the C_{60} model assuming a HI coupling.

The HI coupling in C_{60} is due to intermolecular phonons, describing the rigid vibrations of the C_{60} molecules relative to each other. The coupling to these phonons has usually been assumed to be weak.[30] This is also what we find here. We therefore artificially increase the coupling until λ becomes the same as for the intramolecular coupling. Since $\lambda \sim \omega_{ph}^{-2}$ for intermolecular phonons, we can obtain the increased coupling by artifically reducing the phonon frequency ω_{ph}. Experimentally, the intermolecular frequencies fall in the range from zero and up to almost 7 meV.[31] We have used a value of $\omega_{ph} = 1.8$ meV which is substantially smaller than the average frequency of the experimental spectrum. The resulting $\lambda \sim 0.6$ should therefore be substantially larger than the experimental value.

We compare the resistivity in semiclassical calculations for the C_{60} model with LE and HI coupling in Fig. 7. The same values of $\lambda \sim 0.6$ and $\omega_{ph} = 1.8$ meV were used in both cases. The molecules are orientationally ordered. While the resistivity shows now sign of saturation for the LE coupling (full curve), the model with HI coupling shows a weak saturation (broken curve). This becomes even more pronounced if we neglect the rather trivial temperature dependence of the Fermi-functions in Eq. (14). The resistivity then becomes
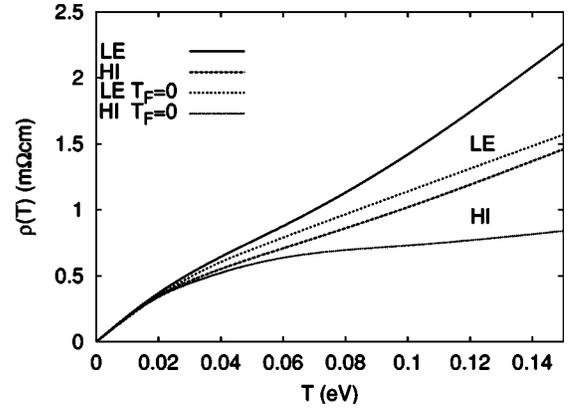

FIG. 7. Resistivity $\rho(T)$ as a function of T for the C_{60} model considering coupling to the level energies (full line, LE coupling) and coupling to the hopping integrals (broken line, HI coupling) according to semiclassical calculations. The C_{60} molecules are ordered. The figure also shows results for the case when the temperature T_F of the Fermi functions in Eq. (14) is put equal to zero. The figure illustrates that there is a large difference between LE and HI coupling for the C_{60} model.

almost constant for HI coupling and large T (dotted curve). For the TM model we find a change of slope in $\rho(T)$ for both HI and LE coupling, but the change is more pronounced for HI coupling.

V. DISCUSSION

A. Loss of Drude peak

We mainly focus on temperatures which are so large that the Drude peak is essentially lost. The Drude peak is related to intraband transitions between states with similar **k** vectors. In Appendix B we illustrate that for Nb_3Sb in the semiclassical approximation, **k** conservation is lost already at rather small values of T and that the concept of intraband transitions becomes rather ill defined. Indeed, for large values of T, it becomes a good approximation to assume that all states couple with the same strength via the current operator to all other states,[12] as is illustrated in Appendix C and in Fig. 8. The Drude peak is then completely lost. Figure 8 shows that for Nb_3Sb the Drude peak is almost completely gone at $T = 0.1$ eV.

B. f-sum rule

In the large-T limit, the f-sum rule provides a very useful tool for analyzing the resistivity. For model Hamiltonians of the type considered here, the f-sum rule takes the form[32] (for a derivation, see Appendix D)

$$\frac{2}{\pi}\int_0^\infty \sigma(\omega)d\omega = -\frac{1}{3}\frac{d^2 e^2}{N\Omega\hbar^2}\langle 0|\hat{T}_K|0\rangle, \qquad (15)$$

where $\hat{T}_K$ is the kinetic energy operator, d is the nearest-neighbor distance, and Ω is the volume per atom. As discussed above, we assume that T is large enough that the Drude peak has been smeared out and that $\sigma(\omega)$ is a smooth function. We furthermore assume that $\sigma(\omega) = 0$ for $\hbar|\omega|$
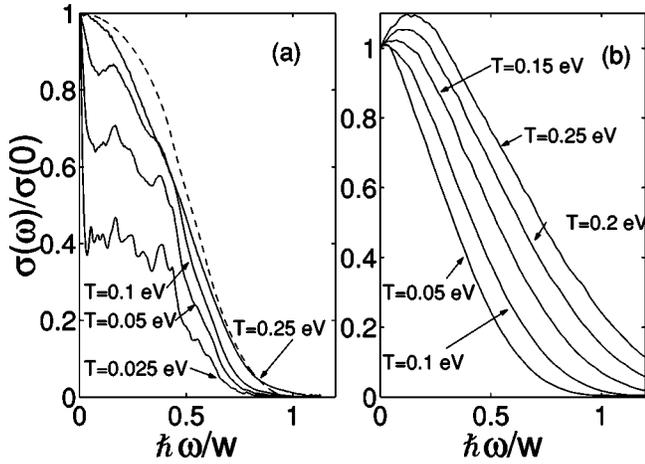
FIG. 8. The optical conductivity as a function of the frequency ω for the (a) $A15$ and (b) C_{60} models in the semiclassical calculation. The frequency has been scaled by the $T=0$ band width W. (a) also shows (broken curve) the result of approximating all current matrix elements by their average [Eq. (C4)].

$>W$, where W is the band width. This is exactly true in the semiclassical treatment and approximately true in the QMC treatment. If $\sigma(\omega) \equiv \sigma(0)$ for $\hbar|\omega| \leq W$, the integral on the left-hand side of Eq. (15) would be $W\sigma(0)/\hbar$ and $\sigma(0)$ would simply be given by this integral multiplied by $\hbar/W$. This is shown schematically in Fig. 9. For a more general shape of $\sigma(\omega)$ we write

$$\sigma(\omega=0) = \frac{\gamma}{W} \int_0^\infty \sigma(\omega)\hbar \, d\omega, \qquad (16)$$

where γ depends on the shape of $\sigma(\omega)$. To estimate γ we assume a certain density of states (DOS) $N(\varepsilon)$ and constant matrix elements of the current operator, as discussed in Appendix C. In Table I we give the value of γ for different shapes of $N(\varepsilon)$, namely, a constant

$$N(\varepsilon) = \begin{cases} \dfrac{1}{W}, & \text{if } |\varepsilon| \leq W/2, \\ 0, & \text{otherwise,} \end{cases} \qquad (17)$$

a Gaussian

$$N(\varepsilon) = \frac{2}{W\sqrt{\pi}} e^{-(2\varepsilon/W)^2} \qquad (18)$$

and a semielliptical

$$N(\varepsilon) = \begin{cases} 8\sqrt{(W/2)^2 - \varepsilon^2}/(\pi W^2), & \text{if } |\varepsilon| \leq W/2, \\ 0, & \text{otherwise.} \end{cases} \qquad (19)$$

DOS. The Table illustrates that γ does not depend strongly on the shape of the DOS. In the following we assume a semielliptical DOS.

It is also interesting to study the filling dependence. This is shown in Table II. The dependence is weak around half-filling, but γ becomes larger for a small filling.
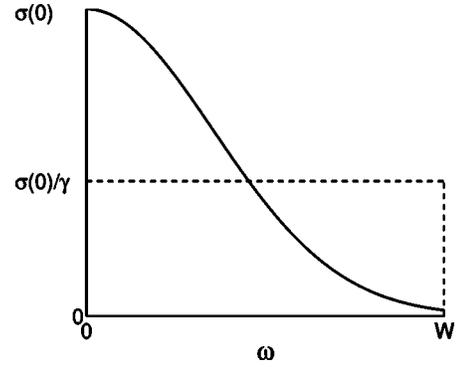

FIG. 9. Schematic picture of $\sigma(\omega)$. The average over the band width is given by $\sigma(0)/\gamma$.

TABLE I. The quantity γ [Eq. (16)] and α [Eq. (20)] for a constant [Eq. (17)], a Gaussian [Eq. (18)] and a semielliptical [Eq. (19)] density of states (DOS) and for half filling.

	Constant	Gaussian	Semielliptical
α	0.125	0.141	0.106
γ	1.44	1.81	1.91
$\alpha\gamma$	0.180	0.255	0.202

C. Large T behavior

As above, we consider temperatures which are so large that the Drude peak is gone, but we furthermore assume that the temperatures are small compared with the band width. This applies, in particular to many transition metal compounds, e.g., the $A15$ compounds. We consider noninteracting electrons, which should be a reasonable assumption for broad band transition metal compounds. To apply the analysis above, we have to calculate the kinetic energy T_K. Since $T \ll W$, we can assume $T=0$ in the calculation of T_K. We find that

$$T_K = 2n \int_{-W/2}^{\mu} \varepsilon N(\varepsilon) d\varepsilon \equiv -2n\alpha WN \qquad (20)$$

is proportional to the band width W and the orbital degeneracy. The shape of the DOS $N(\varepsilon)$ and the filling enter via the parameter α. This parameter is given in Table I for different shapes of the DOS for half filling and in Table II for different fillings and a semielliptical DOS. Inserting the result for T_K in the f-sum rule [Eq. (15)] and using Eq. (16), we obtain

TABLE II. The quantities γ [Eq. (16)] and α [Eq. (20)] for a semielliptical DOS [Eq. (19)] as a function of the fractional filling p. The results are symmetrical around half filling ($p=0.5$).

p	0.1	0.2	0.3	0.4	0.5
α	0.041	0.070	0.090	0.102	0.106
γ	2.63	2.19	2.02	1.93	1.91
$\alpha\gamma$	0.108	0.153	0.182	0.197	0.202

TABLE III. The quantity Ω/d^3 for different lattices, where d is the nearest-neighbor distance and Ω is the volume per atom.

	fcc	bcc	$A15$	sc
Ω/d^3	$\dfrac{1}{\sqrt{2}}=0.707$	$\dfrac{4}{3\sqrt{3}}=0.770$	$\dfrac{4}{3}=1.333$	1

$$\sigma(0) = \frac{\pi\alpha\gamma}{3}\frac{d^3}{\Omega}\frac{ne^2}{\hbar d}. \quad (21)$$

Here $\pi\alpha\gamma/3$ depends on the details of the electronic structure and is of the order of 0.2, d^3/Ω depends on the lattice structure (see Table III), but is of the order 1.

The result (21) is independent of the band width. This follows, since the kinetic energy (20) is proportional to W and is cancelled by the W in Eq. (16).

The quantity $ne^2/(\hbar d)$ has the dimension of a conductivity and it contains the essential material parameters n and d. Here $\hbar a_0/e^2 = 22\ \mu\Omega$cm, where a_0 is the Bohr radius. For a transition metal compound, with $n=5$ and $d\sim 3$ Å, this leads to an upper limit for the resistivity of the order of 0.1–0.2 mΩ cm. This agrees with the saturation resistivities observed for these systems.

It is interesting to study the filling dependence, indicated by Table II. We consider Sc, which is the first element in the $3d$ series. According to a band structure calculation, Sc has about 1.8 $3d$ electrons.[33] Compared with a system close to half filling, such as Nb$_3$Sb, we then expect the saturation resistivity to be about a factor 1.4 larger. This filling effect is somewhat reduced by the different geometries of the compounds. Indeed, while the saturation resistivity is estimated to be 0.15 mΩ cm for Nb$_3$Sb,[1] it is well over 0.2 mΩ cm for Sc,[34] in agreement with the expectations. Similar results are also found for Y.[35] For the other end members of the $3d$, $4d$, and $5d$ series clear saturation does not seem to have been observed.

Using the definition of the mean free path l in the introduction [Eqs. (1)], we can convert the conductivity in Eq. (21) to a mean free path

$$l = cn^{1/3}d, \quad (22)$$

where for simplicity we have assumed that there is only one spherical Fermi surface. For a semielliptical DOS and half filling $c=0.74$ (fcc), 0.72 (bcc), and 0.60 ($A15$). Thus the quantity $cn^{1/3}$ is close to unity for $n=5$, as appropriate here. This provides a quantum-mechanical derivation of the Ioffe-Regel condition for weakly correlated systems.

In particular for the $A15$ lattice, the second nearest neighbor hopping plays a rather important role. The separation $(0.612a)$ is not much larger than for the nearest neighbors $(0.5a)$, but there are eight second nearest neighbors but just two nearest neighbors. For this reason, we also define a distance d which is a weighted average of these distances. As weight factors we use the hopping matrix elements. Thus we define

$$\langle d^2\rangle = \frac{\Sigma_{\mu\nu\sigma}\langle 0|d^2_{\mu\nu}t_{\mu\nu}\psi^\dagger_{\mu\sigma}\psi_{\nu\sigma}|0\rangle}{\Sigma_{\mu\nu\sigma}\langle 0|t_{\mu\nu}\psi^\dagger_{\mu\sigma}\psi_{\nu\sigma}|0\rangle}, \quad (23)$$

where $d_{\nu\mu}$ is the distance between the atoms with the orbitals ν and μ. At $T=0$ this increases d from $0.5a$ to about $0.57a$ for the $A15$ structure. For a semielliptical DOS and filling 0.4, this leads to a larger saturation conductivity and a smaller resistivity of about 0.11 mΩ cm instead of 0.14 mΩ cm if the nearest-neighbor separation is used. This is in better agreement with the calculated resistivity.

In a similar way we can use the f-sum rule to estimate the resistivity for the C$_{60}$ model, although the assumption $T \ll W$ is now much more questionable, as discussed in Sec. V E. Considering a fcc lattice, using $\gamma=1.91$ and $d=10$ Å, we obtain

$$\rho(T) = \frac{0.288}{T_K(T)/(NW)}\ \text{m}\Omega\ \text{cm}. \quad (24)$$

Using the band width $W=0.6$ eV and obtaining $T_K(T)$ from semiclassical calculations for the C$_{60}$ model, we find the saturation resistivity 0.4 mΩ cm. The calculated $\lambda=0$ and $T=0$ resistivity (0.29 mΩ cm) is below this value, while the results for larger values of λ and T strongly exceed the saturation resistivity. The reasons for this are discussed in Sec. V E.

D. Small T behavior

In view of the discussion above, we expect the resistivity to have an upper limit for models with noninteracting electrons scattered by phonons, unless T is very large. In many metals, however, the resistivity increases so slowly with T, that the corresponding conductivity is much large than the limit (21) even at the melting temperature. The issue of whether or not the resistivity saturates is then not raised. It is therefore of interest to study the low-T behavior of $\rho(T)$. For $T>\omega_{ph}$ we expect[18]

$$\rho(T) = 8\pi^2\frac{\lambda Tk_B}{\hbar\Omega^2_{pl}}, \quad (25)$$

where k_B is the Boltzmann constant and λ is the dimensionless electron-phonon coupling constant. For the TM model with HI coupling we define $\lambda = \tilde{\lambda}(\mu,\mu)$, where

$$\tilde{\lambda}(\varepsilon,\varepsilon') = \frac{1}{nKMN(\mu)\omega^2_{ph}}\sum_{ll'i\alpha}\left|\langle l|\frac{\partial H}{\partial R_{i\alpha}}|l'\rangle\right|^2\delta(\varepsilon_l-\varepsilon)$$
$$\times\delta(\varepsilon'_l-\varepsilon'-\omega_{ph}), \quad (26)$$

where K is the number of atoms in a unit cell, the α summation is over the three coordinates, M is the atomic mass, $|l\rangle$ is an eigenstate of H, and i labels the atoms in the unit cell. Ω_{pl} is the plasma frequency

$$(\hbar\Omega_{pl})^2 = \frac{e^2}{3\pi^2}\sum_n\int_{Bz}d^3k\left[\frac{\partial\varepsilon_{n\mathbf{k}}}{\partial\mathbf{k}}\right]^2\delta(\varepsilon_{n\mathbf{k}}-\mu), \quad (27)$$

where $\varepsilon_{n\mathbf{k}}$ is the energy of a state with the band index n and the wave vector $\mathbf{k}$ and μ is the chemical potential. Ω_{pl} depends on the average Fermi velocity.

The straight lines corresponding to Eq. (25) and Eq. (21) are shown in Fig. 3. If these lines cross in the experimentally accessible temperature range we expect saturation.

It is now interesting to compare our models for Nb and Nb_3^*. We obtain similar values of λ for the two cases $\lambda = 1.0$ (Nb_3^*) and $\lambda = 0.9$ (Nb). A larger value of $\lambda = 1.7$ for Nb_3^* was estimated by Allen[3] while a rather similar value was obtained for Nb ($\lambda = 1.0$) from *ab initio* calculations.[36] We observe that $\lambda \sim 1/\omega_{ph}^2$ depends quite sensitively on ω_{ph}. Since we have replaced the whole phonon spectrum by three Einstein phonons per atom, obtained as the average of the phonon spectrum of Nb,[22] one should not expect very accurate values of λ in our calculation. For the plasma frequency we obtain $\Omega_{pl} = 3.6$ eV(Nb_3^*) and 8.2 eV (Nb), in rather good agreement with *ab initio* calculations 3.4 eV (Nb_3^*) (Ref. 37) and 9.5 eV (Nb).[36]

The difference in values of Ω_{pl} for Nb_3^* and Nb alone then leads to a difference by a factor of five in the slope of the line from Eq. (25). As a result Nb_3^* shows a very pronounced saturation already at small T, while Nb only shows sign of saturation at rather large T. The difference is due to the fact that Nb_3^* has a large unit cell with many bands and many forbidden crossings. This leads to quite flat bands and to small electron velocities. The result is a small plasma frequency [Eq. (27)] and a steep line from Eq. (25).

An even more dramatic example is α-Mn, which has a unit cell with 58 atoms.[38] One should therefore expect a very small plasma frequency and a correspondingly early saturation. Indeed, it is found that the resistivity saturates at about $T = 60$ K.[39]

In view of the discussion above, Fig. 8(a) and Eq. (25), it is tempting to write

$$\sigma(\omega = 0, T) = \frac{\hbar \Omega_{pl}^2}{8\pi^2 \lambda T k_B} + \sigma_{sat}, \qquad (28)$$

where the first term describes the Drude peak [Eq. (25)] and the second term is the conductivity in Eq. (21) at saturation. This formula is correct for small T and for T which are so large that the Drude peak is gone but very much smaller than the band width. Eq. (28) is the "parallel resistor" formula of Wiesmann *et al.*[40]

E. Very large T behavior

We have so far discussed temperatures which are so large that the Drude peak have been washed out, but which are small compared with the band width. We now focus on values of T which are large enough that the coupling to the phonons causes a substantial change in the band width. Such effects are not very important for typical transition metal compounds, which have large band widths. They are, however, of substantial interest for the C_{60} model, for which the fluctuations in the level position become comparable to the band width at values of T which can be reached experimentally.

At such large values of T, there is a rather trivial T dependence due to the electron temperature T_F entering in the Fermi functions of Eq. (14). This can be seen by considering the resistivity due to static disorder. Although this scattering mechanism is T independent, the resistivity is, nevertheless, T dependent. Expanding the Fermi functions in Eq. (14) in $1/T$, we obtain that $\sigma(0) \sim 1/T$ and $\rho(T) \sim T$ for very large T. A similar dependence also enters for the the electron-phonon scattering, and it tends to mask some interesting differences between level energy (LE) and hopping integral (HI) couplings. In the following, we therefore freeze the electron temperature, $T_F = 0$, and consider the limit of a very large phonon temperature T_B, i.e., we consider a large T but replace the Fermi functions by Θ functions in Eq. (14).

The band width entering Eq. (16) can be approximately expressed in terms of the second moment of the density of states [Eq. (C9)]. The same is also approximately true for the kinetic energy. We therefore focus on the second moment, which can expressed in terms of the Hamiltonian

$$\langle \varepsilon^2 \rangle = \frac{1}{nN} \sum_{\mu\nu} H_{\mu\nu}^2, \qquad (29)$$

where N is the number of atoms in the system.

We first consider the case of the HI coupling. In our semi-classical formalism we can write

$$\sum_{\mu\nu} H_{\mu\nu}(T) - \sum_{\mu\nu} H_{\mu\nu}(T=0)$$

$$= \sum_{\mu\nu i\alpha} \frac{\partial H_{\mu\nu}}{\partial R_{i\alpha}} \delta R_{i\alpha}(T)$$

$$+ \frac{1}{2} \sum_{\mu\nu i\alpha} \sum_{j\beta} \frac{\partial^2 H_{\mu\nu}}{\partial R_{i\alpha} \partial R_{j\beta}} \delta R_{i\alpha}(T) \delta R_{j\beta}(T) + \cdots, \qquad (30)$$

where the summation over i extends over all atoms. Since the displacements $\delta R_{i\alpha}$ are random, we can assume that

$$\langle \delta R_{i\alpha}(T) \rangle = 0 \quad \langle \delta R_{i\alpha}(T) \delta R_{j\beta}(T) \rangle = \delta_{ij} \delta_{\alpha\beta} \langle R^2 \rangle, \qquad (31)$$

where $\langle R^2 \rangle = k_B T / (M \omega_{ph}^2)$. We then obtain

$$\sum_{\mu\nu} H_{\mu\nu}^2(T) - \sum_{\mu\nu} H_{\mu\nu}^2(T=0)$$

$$= \langle R^2 \rangle \sum_{i\alpha\mu\nu} \left(\frac{\partial H_{\mu\nu}}{\partial R_{i\alpha}} \right)^2 + \langle R^2 \rangle \sum_{\mu\nu i\alpha} H_{\mu\nu} \frac{\partial^2 H_{\mu\nu}}{\partial R_{i\alpha}^2} + \cdots. \qquad (32)$$

Explicit calculations for the TM model show that the second term tend to partially cancel the first term, while for the C_{60} model it adds to the first term. As a crude approximation we neglect the second term. The first term can be approximately related to the electron-phonon coupling λ. Integrating Eq. (26) we obtain

$$NW^2 \lambda \approx \frac{1}{nMN(\mu)\omega_{ph}^2} \sum_{i\alpha\mu\nu} \left(\frac{\partial H_{\mu\nu}}{\partial R_{i\alpha}} \right)^2, \qquad (33)$$
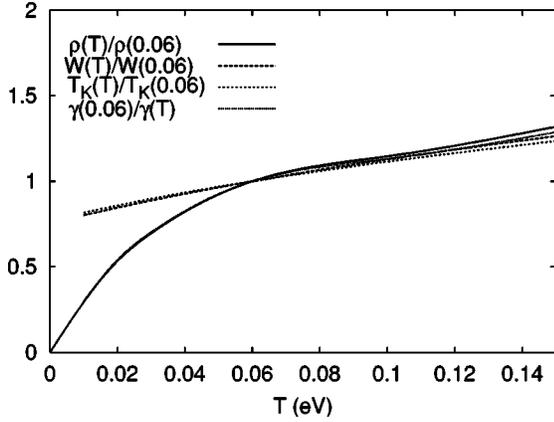
FIG. 10. $\rho(T)$, $T_K(T)$, $W(T)$, and $\gamma(T)$ divided by their $T = 0.06$ eV values for the case of a a coupling to the hopping integrals (HI) in the C_{60} model for $\lambda = 0.6$ and $\omega_{ph} = 0.0018$ eV. The figure illustrates that that the T dependence of $T_K(T)$ and $W(T)$ are similar and therefore to a substantial extent cancel in Eqs. (15), (16) for HI coupling in the C_{60} model, leading to a weak T dependence of $\rho(T)$ for large T. The electron temperature $T_F = 0$ and only the phonon temperature T_B is varied.

where we have assumed that $\tilde{\lambda}(\varepsilon, \varepsilon') \equiv \lambda$. Assuming $N(\mu) = 1/W$, we obtain

$$\sum_{\mu\nu} H_{\mu\nu}^2(T) - \sum_{\mu\nu} H_{\mu\nu}^2(T=0) = nN\lambda W(T=0)k_B T. \quad (34)$$

Assuming that $\langle \varepsilon^2 \rangle = W^2/12$, as is appropriate for a constant density of states, we obtain

$$W(T) = W(0) \sqrt{1 + c_{HI}\lambda \frac{k_B T}{W(T=0)}}, \quad (35)$$

where $c_{HI} = 12$.

We next consider the kinetic energy T_K. As discussed in Sec. V B [Eq. (20)], the kinetic energy is closely related to the band width via the quantity α. As T is increased, however, the shape of $N(\varepsilon)$ changes somewhat, and there is not a perfect proportionality between $W(T)$ and $T_K(T)$. This is illustrated in Fig. 10, where the curves describing the T dependence of these two quantities differ slightly. Nevertheless, from Eqs. (15), (16), it follows that the T dependence of these two quantities largely cancel in the calculation of $\sigma(\omega=0)$ and $\rho(T)$. This is illustrated in Fig. 10, where $\rho(T)$ has only a weak T dependence, once the resistivity has "saturated" (at about $T=0.06$ eV). The remaining T dependence is due to the T dependence of α and γ.

We next consider the case of the LE coupling for the C_{60} model. In this case the second moment is the sum of one contribution from the hopping (off-site elements) of $H_{\mu\nu}$ in Eq. (29) and one contribution from the fluctuations of the level energies (on-site terms) in Eq. (29). Then, at large T,

$$\langle \varepsilon^2 \rangle_T = \langle \varepsilon^2 \rangle_{T=0} + \frac{\lambda}{N(0)} T, \quad (36)$$

where the first term is the off-site and the second the on-site contribution. Assuming a constant $N(\varepsilon)$, we estimate that $T_K(T=0)/N \approx -2.6 \langle \varepsilon^2 \rangle_{T=0}^{1/2}$. For large T, the coupling to the phonons leads to large separations of the levels, and we can use perturbation theory for calculating the kinetic energy.

$$T_K(T) = 2 \sum_{\mu}^{occ} \sum_{\nu}^{unocc} \frac{t_{\mu\nu}^2}{\varepsilon_\mu - \varepsilon_\nu} \approx \frac{1}{2} \frac{Nn\langle \varepsilon^2 \rangle_{T=0}}{\langle \varepsilon_\mu - \varepsilon_\nu \rangle}, \quad (37)$$

where we have replaced the denominator by an average denominator $\langle \varepsilon_\mu - \varepsilon_\nu \rangle$ and the limitations on the sums to occupied and unoccupied states introduce a factor of 1/4. A simple estimate of $\langle \varepsilon_\mu - \varepsilon_\nu \rangle$ is obtained by assuming that the levels have the energies $\pm \Delta\varepsilon/2$. Then the separation of the levels is $\Delta\varepsilon = 2\langle \varepsilon^2 \rangle_T^{1/2}$, where only the on-site contribution to $\langle \varepsilon^2 \rangle$ should be included. At large T, however, the on-site contribution dominates and we have dropped this restriction. Then

$$T_K(T) \approx -2.6N \frac{\langle \varepsilon^2 \rangle_{T=0}}{\langle \varepsilon^2 \rangle_T^{1/2}}, \quad (38)$$

where we have used the same prefactor 2.6 as below Eq. (36). This gives a better agreement with the numerical results than the prefactor (3/4) derived from the arguments above, which is substantially too small, as one would expect. The averaging in Eq. (37) greatly favors small values of the denominator, while our simple estimate focuses on large values. The estimate in Eq. (38) is also a good estimate for $T = 0$, as shown above, and actually for the whole temperature range. As usual, we relate the band width to the second moment. Assuming a constant DOS, Eqs. (15), (16) give

$$\sigma(0) = \frac{2.6\pi\gamma}{6\sqrt{12}} \frac{e^2 d^2}{\Omega\hbar} \frac{\langle \varepsilon^2 \rangle_{T=0}}{\langle \varepsilon^2 \rangle_T}, \quad (39)$$

where one factor $\langle \varepsilon^2 \rangle_T^{1/2}$ comes from the band width and one factor from the kinetic energy. Since $\langle \varepsilon^2 \rangle_T$ grows with T [Eq. (36)], both the kinetic energy and the band width work together to reduce $\sigma(0)$ and to increase $\rho(T)$ as T is increased. Thus we obtain

$$\rho(T) = \frac{0.8}{\gamma(T)} \left(1 + c_{LE}\lambda \frac{T}{W} \right) m\Omega cm, \quad (40)$$

by using parameters appropriate for $A_3 C_{60}$.

From the derivation we obtain $c_{LE} = 12$. A better fit to the data is obtained from $c_{LE} = 15$. In addition we observe that there is also an appreciable T dependence in $\gamma(T)$. These results are illustrated in Fig. 11. In particular, we notice that $W(T)$ and $T_K(T)$ have the opposite T dependence, and therefore work together in the expressions in in Eqs. (15), (16). This is in strong contrast to the case of HI coupling, where the two T dependencies largely cancel each other.

F. Lack of saturation in the C_{60} model

By using the f-sum rule, we showed in Sec. V B that one should expect the resistivity of the alkali-doped fullerenes to saturate at about 0.4 m Ω cm. Actually, this value is almost reach already at $T=0$ (0.3 m Ω) due to the orientational
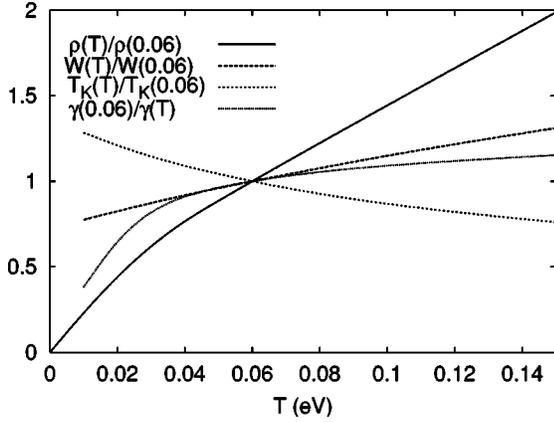
FIG. 11. $\rho(T)$, $T_K(T)$, $W(T)$, and $\gamma(T)$ divided by their $T = 0.06$ eV values for the case of a a coupling to the level energies (LE) in the C_{60} model with $\lambda = 0.6$ and $\omega_{ph} = 0.0018$ eV. The figure illustrates that that the T dependence of $T_K(T)$ and $W(T)$ are the opposite and therefore work in the same direction in Eqs. (15), (16) for the LE coupling in the C_{60} model, leading to a strong T dependence of $\rho(T)$. The electron temperature $T_F = 0$ and only the phonon temperature T_B is varied.

disorder. One can therefore consider the C_{60} model as a case where saturation has already happened at $T = 0$.

This can be further illustrated by considering the resistivity for a model where all the C_{60} molecules have the same orientation, i.e., a system without disorder. The results are compared with the resistivity expected from the Boltzmann equation in Fig. 12. The phonon frequency has been chosen very small, so that the Boltzmann equation gives a linear behavior for all T of interest. For small values of T the Boltzmann equation and the semiclassical theory agree. However, when $\rho(T)$ becomes of the order of 0.3 mΩ cm, shortly before saturation might have been expected, the two curves start to deviate. At this point we may consider the system has having saturated, and the theory in Sec. V E of very large T applies. This theory also predicts a linear behav-
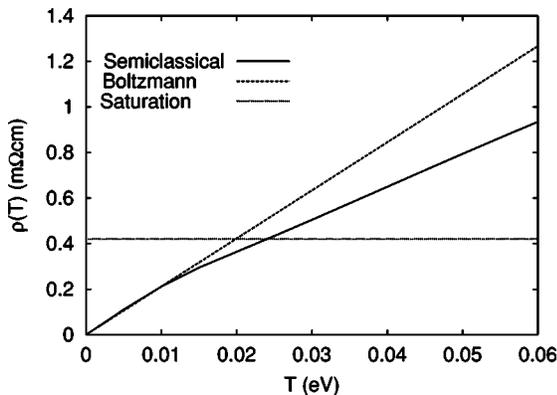

FIG. 12. Resistivity of the ordered C_{60} model for $\omega_{ph} = 0.00001$ eV, $\lambda = 0.6$ and LE coupling. The figure illustrates that the semiclassical (full curve) and the Boltzmann (dashed curve) agree well for small T, but deviates when $\rho(T)$ becomes comparable to the hypothetical saturation resistivity (horizontal dotted curve). The figure shows that there is no real saturation in this case.

ior, but not necessarily with the same slope as at small T. Simple arguments suggest that the two slopes might be of the same order of magnitude, as found in Fig. 12. The small T slope is, however, related to the properties around the Fermi energy, while the very large T slope refers to properties integrated over all states. The two slopes should therefore not be expected to be the same. The Boltzmann equation is not qualitatively wrong for large T in this case, but the relatively good agreement for large T is somewhat accidental.

For the disordered C_{60} model, the disorder itself leads to a resistivity comparable to the "saturation resistivity, and the very large T" limit in Sec. V E applies already for any finite T. This theory predicts that $\rho(T)$ has a linear dependence on T, as is also approximately seen (see Fig. 6). The resistivity could be considered to have "saturated," but this concept is meaningless for the C_{60} model, since the resistivity grows linearly, with a large slope, also after "saturation."

We observe that the boson character of the phonons is important for the arguments in this section and in Sec. V E.[13] Because of this, the number of phonons grow without limit as T is increased, leading to the corresponding growth in the phonon amplitude $\langle R^2 \rangle$. This leads to a continuing growth of the band width and reduction of the kinetic energy for the case of LE coupling. As a result the resistivity does not saturate.

This is different from the case of electron-electron scattering, where Fermi occupation numbers enter the theory. As a result, we have found that there is saturation of the resistivity in a simple one-band, symmetric, half-filled Hubbard model, at least in the dynamical mean-field theory.[13] In view of this, it is interesting that the high-T_c cuprates are usually considered as examples of systems where the resistivity does not saturate, although electron-electron scattering is often believed to be the dominating mechanism. This issue is addressed in the next section.

G. Saturation for high-T_c cuprates

The resistivity in some of the high-T_c cuprates is substantially larger than one would expect from the Ioffe-Regel criterion.[14] It has therefore been assumed that these compounds are examples of systems where the resistivity does not saturate. Using the f-sum rule, however, we have found that the resistivity saturation is to be expected at much higher resistivities than predicted by the Ioffe-Regel criterion or what is found for, e.g., the $A15$ compounds.[14] The reason is that the kinetic energy is strongly reduced in these systems. This is partly due to the strong Coulomb interaction reducing hopping, in particular for systems with a small doping x. Furthermore, only the $x^2 - y^2$ orbital is believed to play an essential role, leading to a small degeneracy $n = 1$. As a result, for $La_{2-x}Sr_xCuO_4$ we find[14]

$$\rho(T) = \frac{0.4}{x(1-x)} \quad m\Omega \text{ cm.} \tag{41}$$

This result is much larger than the saturation resistivity of the order of 0.1 mΩ cm for the $A15$ compounds, in particular for small x. Experimental resistivities are smaller than Eq. (41), but for small values of x not much smaller.[8] For these cases

signs of saturation are indeed seen.[8] We therefore conclude that the data are consistent with saturation. Actually, the data show signs of saturation when the experimental resistivity comes close to the expected saturation resistivity (41).

H. Relation to Mott's minimum conductivity

Within the semiclassical theory, the phonons cause a static disorder. The problem discussed here therefore has some relations to the conduction in disordered system. Thus the LE and HI couplings correspond to diagonal and off-diagonal disorder, respectively. While the disordered systems are usually studied for small T, we are here interested in the large-T behavior. In the semiclassical theory, however, apart from causing disorder, T only enters via the Fermi functions, and it does not play an important role for the qualitative behavior. Below we therefore compare our work with the treatment of disordered systems.

Diagonal disorder can lead to an Anderson metal-insulator transition at $T=0$.[42] For the case of off-diagonal disorder, however, Antoniou and Economou[43] have found that there is no metal insulator transition if the Fermi energy is located in some finite region around the middle of the band. Our semiclassical calculations agree with these results, i.e., we find localization for LE but not for HI coupling as T is increased.

In the QMC calculation of the resistivity, however, we see no sign of localization for LE coupling, just a lack of saturation. This is natural. Localization depends sensitively on the phase factors, which are not destroyed in the elastic scattering in an disordered system. In the inelastic scattering by phonons at finite T these phase factors are, however, lost, and localization is not expected.[42] The effects of the inelastic scattering is properly included in the QMC but neglected in the semiclassical treatment, and therefore localization shows up in the semiclassical but not in the QMC treatment.

Mott[41] has argued that as the disorder increases, there is a discontinuous transition from a metal to an insulator at $T=0$. He therefore introduced the concept of the minimum conductivity

$$\sigma_{\min}=0.026\,\frac{e^2}{\hbar d}, \tag{42}$$

where d is the nearest-neighbor atomic distance. Later work has argued that the transition from a metal to an insulator actually is continuous, but that $\sigma_{\min}$ may still have some relevance for low but nonzero temperatures.[42] We therefore make a comparison of $\sigma_{\min}$ to the resistivity in the TM and C_{60} models. Converting Eq. (42) to a resistivity, we obtain

$$\rho_{\max}=1.6d\quad\text{m}\Omega\text{ cm}, \tag{43}$$

where d is measured in Å. Based on experiment, Mott deduced a somewhat larger minimum conductivity for systems containing transition metal atoms, resulting in the maximum resistivity

$$\rho_{\max}=1\quad\text{m}\Omega\text{ cm}. \tag{44}$$

Mott derived his result for diagonal disorder. His result can most naturally be compared with our saturation resistivity for HI coupling (off-diagonal disorder), since saturation is most pronounced in this case. The resistivity $\rho_{\max}$ is much larger than the saturation resistivity obtained above [Eq. (21)] for the TM model with a fivefold degenerate orbital ($n=5$). For a fcc lattice and a half-filled semielliptical band it takes the form

$$\rho_{\text{sat}}=\frac{0.14d}{n}\quad\text{m}\Omega\text{ cm}, \tag{45}$$

which is of the order of 0.1 mΩ cm.

I. Alternative explanations

Cote and Meisel[6] proposed an interesting explanation of saturation. They argued that the electrons would not see phonons with a wave length Λ that is much longer than the mean free path. They therefore assumed that an electron can only be scattered by a phonon if $l>\Lambda$. As T is increased and l is reduced, an increasing fraction of the phonons become inefficient as scattering sources. The result is that $\rho(T)$ increases much slower than T at large T, in rather good agreement with experiment.[6] We are now in the position to test this assumption.

Above, we have studied a model with three local Einstein phonons on each atom, describing the vibrations in the three coordinate directions. This is equivalent to study Einstein phonons in **q** space. We then write the displacement of the atom at the unperturbed position $\mathbf{R}_i^0$ as

$$\delta\mathbf{R}_l=\frac{1}{\sqrt{N}}\sum_{j\alpha}\mathbf{u}_{j\alpha}e^{i\mathbf{q}_j\cdot\mathbf{R}_l^0}, \tag{46}$$

where $j=1,\ldots,N$ labels the N **q** vectors and α labels the three modes for each **q** vector. The corresponding phonon amplitude is $\mathbf{u}_{j\alpha}$. We perform a calculation where the phonons are treated semiclassically as before, but where the amplitudes $\mathbf{u}_{j\alpha}$ are treated as random variables. This gives the same resistivity as before. We then gradually turn off the long wave length phonons, putting the corresponding amplitudes $\mathbf{u}_{j\alpha}=0$. For small T we expect this to reduce the resistivity. For large T, however, the arguments of Cote and Meisel[6] suggests that this should not influence the resistivity if $\Lambda>l$ for the phonons turned off.

We group the **q** vectors with equal length in shells. Shells with **q** vectors of similar length are further grouped together in such way that each group contains a similar number of **q** vectors. Then the groups of phonons are successively turned off. The results are shown in Fig. 13. The figure illustrates that as a group of phonons is turned off there is a drop in the resistivity. This is not only true for small T but for all T studied here. Consider for instance the curve with all phonons included and $T=0.4$ eV. The resistivity $\rho\sim0.1$ mΩ cm corresponds to $l\sim3.5$ Å. The theory of Cote and Meisel then assumes that all phonons with $\Lambda>3.5$ Å can be turned off without ρ changing. The figure illustrates that this is far from the result of our calculation. This illustrates that also phonons with a relatively long wave length contribute substantially to the large-T resistivity, although $\Lambda>l$.
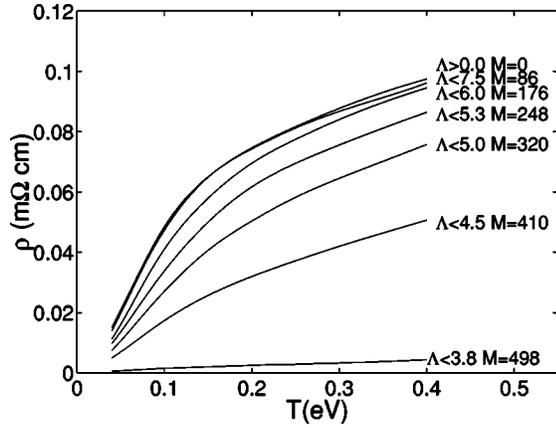
FIG. 13. The resistivity of Nb as a function of T. The scattering from phonons of successively shorter and shorter wave lengths Λ is suppressed. For the uppermost curve all phonons are considered. In the lower curves the phonons corresponding to the M shortest **q** vectors (longest wave lengths) were suppressed, where M is marked at the curve. The figure illustrates that the long wave length phonons contribute about equally much both to the small T resistivity and large T resistivity.

Figure 13 illustrates that phonons with a very long wave length make a small contribution to the resistivity for any T. The reason is that a long wave length phonon does not change the relative separation of two neighboring atoms very much, which means that the corresponding hopping matrix element is not changed very much.

It has also been argued[44] that resistivity saturation can be understood in a Holstein model, somewhat similar to our C_{60} model. For small T and large λ the Holstein model shows an "excess" resistivity. Similar effects are observed in our C_{60} model, as is seen in Fig. 6 for $\lambda = 0.80$. The result is that the slope of the $\rho(T)$ curve is reduced as T is increased. To analyze this, we compare the calculated $\rho(T)$ with the resistivity

$$\rho(T) = 0.29 + 17\lambda T \quad \text{m}\Omega \text{ cm}, \qquad (47)$$

in Fig. 14. The value 0.29 comes from the orientational disorder and the term $\sim \lambda T$ is the type of behavior we expect for a normal nonsaturating system (e.g., from Boltzmann theory). The slope was adjusted to the results for $\lambda = 0.26$. For such a small value of λ there is no sign of saturation in Fig. 6. If the system shows saturation for larger values of λ, we would then expect the calculated resistivity to be below Eq. (47). We find, however, that QMC results for large T stay above these results for all values of λ that we have studied. In the figure this is illustrated for $\lambda = 0.8$. As pointed out in Ref. 44, the resistivity in this model actually does not saturate, and it was concluded that "saturation" is a misnomer. As we have shown above, however, the TM model is a much better model of saturation, both because it is much more realistic for systems showing saturation, and because it also gives results much more similar to experiment.

In a semiclassical treatment of the type used by Millis *et al.*[44] the "excess" resistivity for large λ and small T is due to the formation of a highly anharmonic potential well for
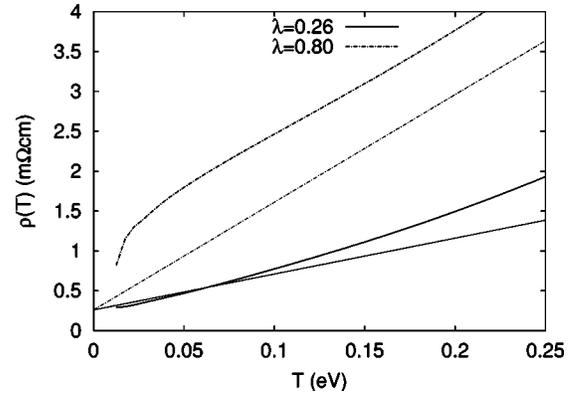

FIG. 14. Resistivity $\rho(T)$ as a function of temperature T and electron-phonon coupling λ for the C_{60} model according to QMC calculations. The phonon frequency is $\omega_{ph} = 0.1$ eV. The straight lines show the resistivity $\rho(T) = 0.29 + 17\lambda T$ mΩ cm, where 0.29 is the resistivity due to the orientational disorder. The figure illustrates that there is some "excess" resistivity at moderate T and large λ but no saturation for this model.

the phonons. This leads to a larger vibration amplitude and an increased resistivity. Similar results are found in our QMC calculation, as discussed above. In a more realistic model, the electrons would couple to many phonon modes, each typically with a substantially weaker coupling. Even if the total λ may be large, each phonon would in such a model have a more harmonic potential well, and we would not expect a large "excess" resistivity. This further supports our belief that this type of model is not appropriate for describing resistivity saturation.

VI. SUMMARY

We have studied models of weakly correlated transition metal compound (TM model) and of alkali-doped fullerenes (C_{60} model). These models were studied using Quantum Monte Carlo (QMC) and semiclassical methods. The results, as well as earlier results for the high-T_c cuprates, were analyzed by using the f-sum rule. We assumed that T is so large that the Drude peak has been smeared out. Then [Eqs. (15), (16)] an approximate lower limit to $\sigma(0)$ is given by

$$\frac{1}{\rho(T)} = \sigma(0) \sim \frac{1}{W} \int_0^\infty \sigma(\omega) d\omega \sim \frac{|T_K(T)|}{dW(T)}, \qquad (48)$$

where $T_K(T)$ is the kinetic energy, $W(T)$ is the band width, and d is the nearest neighbor distance.

We first considered $T \ll W$. For the TM model of noninteracting electrons, it then followed that $T_K \sim W$. This leads to the simple upper limit

$$\sim \frac{\hbar d}{ne^2} \qquad (49)$$

for the resistivity, where $n=5$ is the orbital degeneracy of the d level. This agrees rather well with the saturation resistivity of many transition metal compounds, and it corresponds to a mean free path $l \sim d$.

For the high-T_c compounds, the kinetic energy is strongly reduced by correlation effects. There is a strong reduction in the hopping probability of an electron to a neighboring site if there already is an electron on this site. This leads to $|T_K| \sim x(1-x)$, where x is the doping. The corresponding upper limit for the resistivity is then

$$\sim \frac{\hbar c}{e^2 x(1-x)}, \tag{50}$$

where c is the distance between two CuO_2 planes. Since essentially only the x^2-y^2 orbital is involved, the degeneracy factor is $n=1$. This resistivity is much larger than for the TM model, both because of $n=1$ and because of factor $x(1-x)$. This limit is therefore apparently never exceeded for any high-T_c compound. There are only a few cases where the resistivity gets close to this limit, and in these cases the resistivity shows signs of saturation.

Whether or not saturation is actually observed, depends on how rapidly the resistivity grows for small T's. In this limit we have $\rho(T) \sim \lambda T/\Omega_{pl}^2$ for the TM model. For the $A15$ compounds, e.g., Nb_3Sn, λ is fairly large and Ω_{pl} is very small, due to the large unit cell and the quite flat bands. The result is that the resistivity grows very rapidly for small T and gets close to the limiting value for rather small T. The resistivity then shows a pronounced saturation. For Nb, on the other hand, Ω_{pl} is much larger and the resistivity grows much more slowly with T, and there is only a weak saturation. For most metals, the limiting resistivity would only be reached far above the melting temperature, due to the slow increase of $\rho(T)$ for small T.

We also considered very large values of T, where T becomes comparable to the band width. Then both T_K and W have strong T dependences. It is important to distinguish between the case when the phonons couple to the level positions (LE coupling) and to the hopping integrals (HI coupling). In the former case, T_K decreases with T, since the different levels have different energies, and hopping is reduced. In the latter case, T_K is increased, since the square of the hopping integrals increases with T. In both cases W increases with T. In the LE case, both effects work together [Eq. (48)] to reduce $\sigma(0)$ and to increase the resistivity. In the HI case, on the other hand, the two effects partly compensate each other, and the increase in the resistivity is smaller.

These considerations are very relevant for the C_{60} case. Due to the orientational disorder, the saturation limit can be considered to have been reached already for $T=0$. Because of the the small band width, however, the T dependence of the band width and the kinetic energy become very important. Furthermore, the coupling is of the LE type, so that the T dependence of these two quantities cooperate in increasing the resistivity. The result is a drastic increase in the resistivity, beyond the "saturation resistivity," and little or no sign
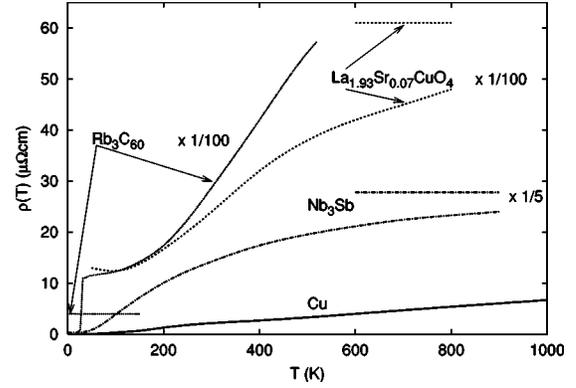

FIG. 15. Resistivity of Cu, Nb_3Sb (multiplied by a factor 1/5) (Ref. 1), $La_{1.93}Sr_{0.07}CuO_4$ (multiplied by 1/100) (Ref. 8), and alkali-doped C_{60} (multiplied by 1/100) (Ref. 9). The figure also shows our estimated saturation resistivities for the latter three cases. The figure illustrates that the resistivity saturates for Nb_3Sb and $La_{1.93}Sr_{0.07}CuO_4$ but not for alkali-doped C_{60}.

of saturation. We may therefore consider C_{60} to belong to a different class than the $A15$ and high-T_c compounds.

This is illustrated in Fig. 15, which shows the resistivity for Cu, Nb_3Sb, $La_{1.93}Sr_{0.07}CuO_4$, and hole-doped C_{60}, where the resistivities of the latter three metals have been reduced by factors 5, 100, and 100. The resistivities of Nb_3Sb and $La_{1.93}Sr_{0.07}CuO_4$ stay below the expected saturation resistivities, while the resistivity of C_{60} is far above the "saturation" resistivity, shown in the lower left corner of the figure. This suggests that the systems studied here fall in three different classes, namely, (i) weakly correlated transition metal compounds, showing saturation in agreement with the Ioffe-Regel condition, (ii) strongly correlated high-T_c cuprates, showing saturation but at much larger values than predicted by the Ioffe-Regel condition, and (iii) alkali-doped C_{60} compounds, showing no saturation.

APPENDIX A: QMC FOR THE TM MODEL

The Hamiltonian of the TM model can be written as

$$H = \sum_{\mu,\nu} H_{\mu,\nu} = \sum_{\eta=1}^{N_b} H_\eta, \tag{A1}$$

where η labels a given ordering of the $N_b=zNn^2$ bonds, z being the number of atoms connected to a given site by the Hamiltonian operator.

Defining $\Delta\tau=\beta/L$, using Trotter decomposition at lowest order and breaking up the Hamiltonian in N_b terms, the partition function is,[45]

$$Z = \text{Tr}\left[\prod_{l=1}^{L} e^{-\Delta \tau H}\right] \simeq \text{Tr}\left[\prod_{l=1}^{L} \prod_{\eta=N_b}^{1} e^{-\Delta \tau H_\eta}\right]. \quad (A2)$$

Integrating out the electron degrees of freedom[15] leads to

$$Z = [\det(1 + B_L B_{L-1} \cdots B_1)]^2 \quad (A3)$$

with

$$B_l = \prod_{\eta=N_b}^{1} b_\eta^l = \prod_{\eta=N_b}^{1} e^{-\Delta \tau H_\eta}. \quad (A4)$$

The matrices b_η^l have dimension Nn and have the following form:

$$b_\eta^l = \begin{pmatrix} 1 & .. & & 0 & .. & & 0 & .. & 0 \\ : & : & & : & : & & : & : & : \\ 0 & .. & \cosh(\Delta \tau H_\eta) & .. & \sinh(-\Delta \tau H_\eta) & .. & 0 \\ : & : & & : & : & & : & : & : \\ 0 & .. & \sinh(-\Delta \tau H_\eta) & .. & \cosh(\Delta \tau H_\eta) & .. & 0 \\ : & : & & : & : & & : & : & : \\ 0 & .. & & 0 & .. & & 0 & .. & 1 \end{pmatrix}. \quad (A5)$$

It can be shown[15] that the electron Green function is written as

$$g = (1 + B_L \cdots B_2 B_1)^{-1}. \quad (A6)$$

During the simulation, g and g^{-1} are constantly stored and updated.

A quantum Monte Carlo move is a displacement of a phonon coordinate for a given slice. The move is then accepted or rejected according to the Metropolis algorithm which involves the calculation of the square determinant ratio between the electron Green functions after and before the displacement, $R^2 = [\det(g')/\det(g)]^2$.

Without loss of generality let us suppose that an atom i is displaced in the first slice (so that we can omit the higher index in b_η^l). This will involve a change in $B_1 \to B_1'$ or $N_c = zn^2$ changes in the factors

$$b_{i_k} \mapsto b_{i_k}' = b_{i_k} \Delta_{i_k}, \quad k = 1, 2, \ldots, N_c \quad (A7)$$

with $\{i_1 < i_2 < \cdots < i_{N_c}\}$. In the case only one b_{i_1} factor is changed ($N_c = 1$) the determinant ratio can be easily obtained as

$$R = \frac{\det(1 + B_L \cdots B_2 b_{N_b} \cdots b_{i_1} \Delta_{i_1} \cdots b_1)}{\det(1 + B_L \cdots B_2 B_1)} \quad (A8)$$

$$= \det[1 + (1 - \bar{g}_1)(\Delta_{i_1} - 1)], \quad (A9)$$

where $\bar{g}_1 = (1 + b_{i_1} \cdots b_1 B_L \cdots B_2 b_{N_b} \cdots b_{i_1})^{-1}$ is a modified electron Green function and is obtained from g as

$$\bar{g}_1 = (b_{i_1-1} \cdots b_1) g (b_{i_1-1} \cdots b_1)^{-1}. \quad (A10)$$

The matrix $(\Delta_j - 1)$ is symmetric and has only four matrix elements different from zero, as can be seen from Eq. (A5), (A7), so that the products in Eq. (A9) can be performed in order Nn operation.

So far it is known how to calculate the determinant as long as a single bond is changed. In the more complicate case of several bonds, the problem can be reduced to this simpler one by noting that the determinant is expressed as

$$R = R_{N_c, N_c-1} R_{N_c-1, N_c-2} \cdots R_{1,0} \quad (A11)$$

and $R_{j,j-1}$ is the ratio between two determinants having changed only the first j and $j-1$ bonds, respectively,

$$R_{j,j-1}$$
$$= \frac{\det(1 + B_L \cdots B_2 b_{N_b} \cdots b_{i_j} \Delta_{i_j} \cdots b_{i_1} \Delta_{i_1} \cdots b_1)}{\det(1 + B_L \cdots B_2 b_{N_b} \cdots b_{i_{j-1}} \Delta_{i_{j-1}} \cdots b_{i_1} \Delta_{i_1} \cdots b_1)}. \quad (A12)$$

Each of these N_c determinant ratios is given by Eq. (A9) with the Green function g replaced by the new one

$$\bar{g}_{j-1} = (1 + b_{i_j-1} \cdots b_{i_{j-1}}' \cdots b_{i_1}' \cdots b_1' B_L \cdots b_2 b_L \cdots b_{i_j})^{-1} \quad (A13)$$

which has only the first $j-1$ bonds updated.

Once the determinant $R_{j,j-1}$ has been obtained, it is necessary to update the Green function $\bar{g}_{j-1}$ to the new one $\bar{g}_j$ which will be used to evaluate $R_{j+1,j}$. This update is done in two steps and requires the knowledge of $\bar{g}_j^{-1}$ so that the function g^{-1} has to be bookkeeped during the simulation.

The first step is to define the new Green function $\tilde{g}_j$ as

$$\tilde{g}_j = (1 + b_{i_j-1} \cdots b_{i_{j-1}}' \cdots b_{i_1}' \cdots b_1' B_L \cdots b_2 b_L \cdots b_{i_j}')^{-1}. \quad (A14)$$

$\tilde{g}_j$ differs from $\bar{g}_{j-1}$ only by the substitution $b_{i_j} \to b'_{i_j}$. It can be obtained using the Green function updating in the simpler case of a single bond change,[15] namely,

$$\tilde{g}_j = [\bar{g}_{j-1}^{-1} + (\bar{g}_{j-1}^{-1} - 1)(\Delta_{i_j} - 1)]^{-1}. \tag{A15}$$

The matrix $A = (\bar{g}_{j-1}^{-1} - 1)(\Delta_{i_j} - 1)$ is zero everywhere a part from two columns. As a consequence, Eq. (A15) can be efficiently performed with the Shermann-Morrison formula[46] applied to $\bar{g}_{j-1}^{-1}$ so that the calculation of $\tilde{g}_j$ involves order $(Nn)^2$ operations.

The second step is then to obtain from $\tilde{g}_j$ the Green function $\bar{g}_j$ as follows:

$$\bar{g}_j = (b_{i_{j+1}-1} \cdots b_{i_j+1} b'_{i_j}) \tilde{g}_j (b_{i_{j+1}-1} \cdots b_{i_j+1} b'_{i_j})^{-1}. \tag{A16}$$

Once $\bar{g}_j$ is known it is clearly possible to obtain $R_{j+1,j}$ following the same steps we have outlined before.

For a given Trotter slice and a given phonon coordinate the algorithm can be summarized as follows

(1) Displace coordinate $R_i \to R'_i$ and identify the bonds $i_1 < i_2 < \cdots < i_{N_c}$ which will be affected by the atomic displacement.

(2) Set $\tilde{g}_0 = g$ and $\tilde{g}_0^{-1} = g^{-1}$, compute $\bar{g}_0$ and $\bar{g}_0^{-1}$ using Eq. (A16) and the similar one for $\bar{g}_0^{-1}$.

(3) Perform loop $j = 1, \ldots, N_c$ over the previously identified bonds.

(4) Calculate the matrix Δ_{i_j}.

(5) Calculate $R_{j,j-1}$ using $\bar{g}_{j-1}$ and Eq. (A9).

(6) Update $\bar{g}_{j-1} \to \bar{g}_j$ and $\bar{g}_{j-1}^{-1} \to \bar{g}_j^{-1}$ using Eqs. (A15), (A16).

(7) End loop over j.

(8) Compute R and check if the proposal move is accepted.

(9) If the proposal is accepted update $\bar{g}_{N_c-1} \to \tilde{g}_{N_c}$ from Eq. (A15).

After the proposed displacement for atom i has been accepted by the Metropolis condition, the most straightforward way to proceed would be to obtain the new Green function g' [Eq. (A6)], with all the b_η factors updated, as

$$g' = (b_{i_{N_c}} \cdots b_1)^{-1} \tilde{g}_{N_c} (b_{i_{N_c}} \cdots b_1) \tag{A17}$$

and then from step 2 of the algorithm obtain the new $\bar{g}_0'$ for the atom $j = i + 1$. Note anyway that these two steps can be efficiently condensed in one if a particular order for the sites is chosen. If the sites are ordered in such a way that i_1 increase monotonically with i, e.g., $\{1_1 < 2_1 < \cdots < N_{c_1}\}$, then Eq. (A17) becomes

$$\tilde{g}_0' = (b_{i_{N_c}} \cdots b_{j_1})^{-1} \tilde{g}_{N_c} (b_{i_{N_c}} \cdots b_{j_1}) \tag{A18}$$

involving $2j_{i_1}$ products by b_η factors less than the most straightforward procedure.

APPENDIX B: LOSS OF MOMENTUM CONSERVATION

At large T the phonon vibrations become very large. In the semiclassical treatment of the phonons, this tends to destroy the periodicity and therefore it tends to violate momentum conservation within the electronic system. Below we test how this violation increases with T in the TM model using a HI coupling. Qualitatively similar results are, however, obtained also in the other models. We first calculate the states of the Hamiltonian at $T = 0$. The system is then perfectly periodic and all the states $|n\mathbf{k}, T = 0\rangle$ can be labeled by a wave vector $\mathbf{k}$ and a band index n. We use a unit cell with six Nb atoms and the band index therefore runs over 30 states. Next the states at a finite T are calculated. These states $|l, T\rangle$ are labeled by an index l. These states can be expanded in the complete set of $T = 0$ states

$$|l, T\rangle = \sum_{\mathbf{k}n} |n\mathbf{k}, T = 0\rangle \langle n\mathbf{k}, T = 0 | l, T\rangle. \tag{B1}$$

For a given state we determine the amount of $\mathbf{k}$ character

$$c_{\mathbf{k}}(l) = \sum_n |\langle n\mathbf{k}, T = 0 | l, T\rangle|^2 \tag{B2}$$

or the amount of mixing with states having the band index n

$$c_n(l) = \sum_{\mathbf{k}} |\langle n\mathbf{k}, T = 0 | l, T\rangle|^2. \tag{B3}$$

From normalization it follows that $\Sigma_{\mathbf{k}} c_{\mathbf{k}}^{(l)} = 1$ and $\Sigma_n c_n^{(l)} = 1$. We define

$$\Delta_k(l) = n_{\mathbf{k}} \sum_{\mathbf{k}} [c_{\mathbf{k}}^{(l)}]^2 \tag{B4}$$

and

$$\Delta_n(l) = 30 \sum_n [c_n^{(l)}]^2, \tag{B5}$$

where $n_{\mathbf{k}}$ is the number of allowed $\mathbf{k}$ vectors and 30 is the number of band index. If the weight of a given state l is equally distributed over $n_{\mathbf{k}}/m$ different $\mathbf{k}$ vectors, $\Delta_k(l) = m$. In particular, if all effects of periodicity are lost, we expect that $\Delta_k(l) = 1$, since we then expect all $n_{\mathbf{k}}$ $\mathbf{k}$ components to have equal weight ($m = 1$). On the other hand, if a state contains only one $\mathbf{k}$ vector, $\Delta_k(l) = n_{\mathbf{k}}$. Typically in the periodic system, several states with different $\mathbf{k}$ vectors are degenerate, e.g., states with $\mathbf{k}$ and $-\mathbf{k}$ may be degenerate. Even at a very small amount of disorder, a state of the disordered system is then typically a linear combination of states with several different $\mathbf{k}$ vectors, and $\Delta_k(l)$ is reduced correspondingly. We consider a super cell with periodic boundary conditions. The value of $n_{\mathbf{k}}$ then depends on the size of the supercell. For a given amount of disorder, we expect that a given state will contain $\mathbf{k}$ vectors from a certain fraction of the Brillouin zone. The number of $\mathbf{k}$ vectors increases with the size of the supercell. However, m introduced above should stay roughly constant. Thus we find that definition (B4) gives results which are rather independent of the
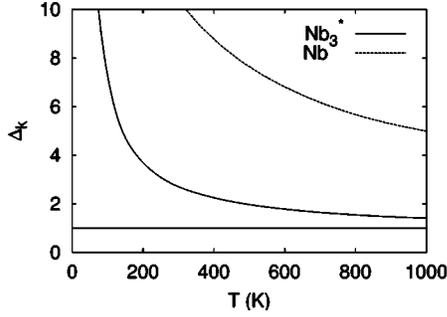
FIG. 16. The quantity Δ_k in Eq. (B6) for Nb_3^* and Nb as a function of T for $n_k = 256$ allowed **k** vectors. Δ_k measures the loss of periodicity. The horizontal line ($\Delta_k = 1$) represents complete loss of periodicity. The figure illustrates the rapid loss of periodicity and momentum conservation for the Nb_3^* model, while this loss happens more slowly for Nb.

super cell size for values of T which are not very small. On the other hand, for $T \approx 0$, this definition gives results which grow roughly linearly with n_k. The definition is, however, sensible for the range of T of interest here. In a similar way it follows that $\Delta_n(l) = 1$ if the conservation of the band indices is completely lost.

We average over all states

$$\Delta_i = \sum_l \Delta_i(l)/(Nn), \quad i = k \quad \text{or} \quad n. \quad \text{(B6)}$$

Figure 16 shows Δ_k for Nb_3^* and Nb, where Δ is an average over $\Delta(l)$. The line $\Delta = 1$, corresponding to a complete loss of periodicity, is also shown. The figure illustrates that for Nb_3^* much of the periodicity is lost already for $T \sim 200 - 300$ K. For Nb this happens at higher T, but also in this case periodicity is lost fairly quickly.

The rapid loss of periodicity for Nb_3^* can be related to the many flat bands. This means that there are states with all **k** values within a rather small energy range. Then only a small perturbation is needed to mix all these different **k** values, implying a loss of momentum conservation.
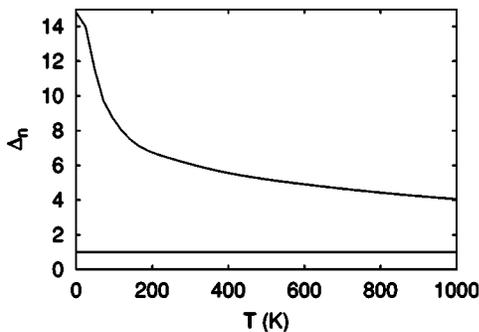
In a similar way, Fig. 17 shows that the meaning of the

band indices is lost relatively quickly for Nb_3^* as T is increased. Therefore the meaning of intraband and interband transitions is lost.

APPENDIX C: CONSTANT CURRENT MATRIX ELEMENTS

In view of the rapid loss of momentum conservation, illustrated in Appendix B, it is interesting to consider the limit where momentum conservation is completely lost due to the disorder. This is the opposite limit to the traditional Bloch-Boltzmann treatment, where the scattering is assumed to be so small that **k** is a useful quantum number. In the complete disorder limit studied here, all states are coupled to all states via the current operator. The calculations for the Nb_3^* model show that these assumptions, taken literally, are not satisfied. We note, however, that the expression in Eq. (14) for the optical conductivity can be rewritten as

$$\sigma(\omega) = \frac{2\pi n^2}{N\Omega\omega} \int d\varepsilon N(\varepsilon) \int d\varepsilon' N(\varepsilon') j(\varepsilon, \varepsilon')$$

$$\times [f(\varepsilon) - f(\varepsilon')] \delta(\hbar\omega - \varepsilon' + \varepsilon), \quad \text{(C1)}$$

where

$$j(\varepsilon, \varepsilon') = \frac{1}{n^2 N(\varepsilon) N(\varepsilon')}$$

$$\times \sum_{ll'} |\langle l|j_x|l'\rangle|^2 L(\varepsilon - \varepsilon_l) L(\varepsilon' - \varepsilon_l'), \quad \text{(C2)}$$

$N(\varepsilon)$ is the density of states per atom, orbital, and spin, and n is the orbital degeneracy. $L(\varepsilon) = (\gamma/\pi)/(\varepsilon^2 + \gamma^2)$ is a Lorentzian. The function $j(\varepsilon, \varepsilon')$ is shown in Fig. 18 for two values of T, using the broadening $\gamma = 0.01$ eV. The figure illustrates that the function $j(\varepsilon, \varepsilon')$ has only a moderate dependence on the energies for $T = 0.043$ eV $= 500$ K. We
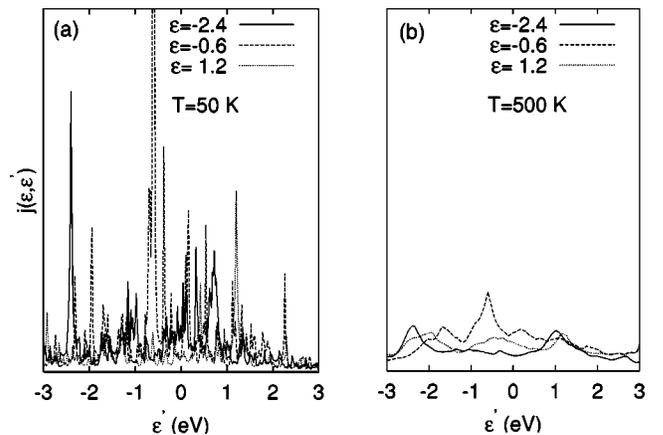

FIG. 18. Average $j(\varepsilon, \varepsilon')$ of the current matrix elements over states with similar energies [Eq. (C2)] for Nb_3^*. The units are arbitrary. The figure illustrates that for $T = 0.0043$, eV $= 50$ K $j(\varepsilon, \varepsilon')$ varies strongly with the energies while for $T = 0.043$, eV $= 500$ K this variation is much less pronounced.

FIG. 17. The quantity Δ_n in Eq. (B6) for Nb_3^* as a function of T for $n_k = 256$ allowed **k** vectors. Δ_n measures how the conservation of the band index is lost, with the horizontal line ($\Delta_n = 1$) showing a complete loss. The figure illustrates how the meaning of the band indices is lost relatively rapidly for the Nb_3^* model.

therefore now work out the consequences of assuming that the matrix elements of the current can be replaced by their average.

This average is defined as

$$j_{\rm av}^2 = \frac{1}{(Nn)^2} \sum_{ll'} |\langle l|\hat{j}_x|l'\rangle|^2, \qquad (C3)$$

where $|i\rangle$ are the Nn eigenstates of the Hamiltonian. The expression (14) for the optical conductivity can then be written as

$$\sigma(\omega) = \frac{2\pi}{N\Omega} j_{\rm av}^2 \sum_l^{\rm occ} \sum_{l'}^{\rm unocc} \frac{1}{\omega} \delta(\hbar\omega - \varepsilon_{l'} + \varepsilon_l), \qquad (C4)$$

where we have considered $\omega > 0$ and assumed that $T \ll W$ so that we can replace the Fermi functions by Θ functions. Figure 8(a) compares the actually calculated $\sigma(\omega)$ with the result of (C4), assuming a semielliptical DOS [Eq. (C4)]. The good agreement for large T gives further justification for the assumptions behind Eq. (C4). This gives

$$\sigma(\omega=0) = \frac{2\pi N n^2 \hbar}{\Omega} j_{\rm av}^2 N(\mu)^2, \qquad (C5)$$

where μ is the chemical potential. We then need to find a relation between $j_{\rm av}$ and $N(\mu)$, which is obtained from charge and current conservation. We first rewrite $j_{\rm av}$ as

$$j_{\rm av}^2 = \frac{1}{(Nn)^2} \sum_{\nu\mu} |\langle \nu|\hat{j}_x|\mu\rangle|^2, \qquad (C6)$$

where $|\nu\rangle$ is a basis state in a local representation. We then use the charge and current conservation in Eq. (5), relating the current and hopping matrix elements. This gives

$$\sum_{\alpha=x,y,z} |\langle \nu|\hat{j}_\alpha|\mu\rangle|^2 = \frac{e^2 d^2}{\hbar^2} t_{\nu\mu}^2 \qquad (C7)$$

and for an isotropic system

$$j_{av}^2 = \frac{1}{(Nn)^2} \frac{e^2 d^2}{3\hbar^2} \sum_{\nu\mu} t_{\nu\mu}^2. \qquad (C8)$$

To relate j_{av}^2 to $N(\varepsilon)$, we introduce the second moment

$$\langle \varepsilon^2 \rangle = \int_{-\infty}^{\infty} N(\varepsilon)\varepsilon^2 d\varepsilon, \qquad (C9)$$

where $N(\varepsilon)$ is normalized to unity. This quantity can be related to the hopping integrals

$$n\langle \varepsilon^2 \rangle = \frac{1}{N} \sum_{\nu\mu} t_{\nu\mu}^2. \qquad (C10)$$

We assume a specific form for $N(\varepsilon)$, calculate $\langle \varepsilon^2 \rangle$ for this form and then relate it to $N(\mu)$. Table IV shows results for different shapes of the DOS. The table illustrates that there is not a drastic dependence on the shape of $N(\varepsilon)$. In the following, we focus on the semielliptical DOS, which is probably the most realistic one of the three cases considered.

TABLE IV. The quantity $\langle \varepsilon^2 \rangle N(\mu)^2$ for a constant [Eq. (17)], a Gaussian [Eq. (18)] and a semielliptical [Eq. (19)] density of states (DOS) and for half filling.

	Constant	Gaussian	Semielliptical
$\langle \varepsilon^2 \rangle N(\mu)^2$	$\dfrac{1}{12} = 0.083$	$\dfrac{1}{2\pi} = 0.159$	$\dfrac{1}{\pi^2} = 0.101$

Expressing $\Sigma t_{\nu\mu}$ in terms of $\langle \varepsilon^2 \rangle$ in Eq. (C8), we can rewrite Eq. (C5) as

$$\sigma(0) = \frac{2\pi n}{3} \frac{d^3}{\Omega} \langle \varepsilon^2 \rangle N(\mu)^2 \frac{e^2}{d\hbar}, \qquad (C11)$$

where Ω/d^3 is shown in Table III. The quantity $e^2/(\hbar d)$ has the unit of conductivity and Eq. (C11) can be rewritten as

$$\rho = \frac{1}{\sigma(0)} = 19.7 \frac{\Omega/d^3}{\langle \varepsilon^2 \rangle N(\mu)^2} \frac{d}{n} \mu\Omega\,{\rm cm}, \qquad (C12)$$

where d is now expressed in Å. As seen in Tables IV and III, $\langle \varepsilon^2 \rangle N(\mu)^2 \sim 0.1$ and $\Omega/d^3 \sim 1$. For a transition metal, we may use $d \sim 3$ Å and $n = 5$, which leads to $\rho \sim 100\ \mu\Omega$ cm. Such a resistivity is indeed typical for the saturation resistivity of a transition metal compound.

APPENDIX D: DERIVATION OF THE f-SUM RULE

In this appendix we derive the f-sum rule, essentially following Maldague.[32] We introduce the position operator

$$\hat{R}_x = \sum_{\nu\sigma} R_x^\nu \psi_{\nu\sigma}^\dagger \psi_{\nu\sigma}. \qquad (D1)$$

For tight-binding Hamiltonians and when the current operator has no on-site matrix elements

$$\hat{j}_x = \frac{ie}{\hbar}[\hat{R}_x, H]. \qquad (D2)$$

For $\omega > 0$, the optical conductivity is written as

$$\sigma(\omega) = \frac{\pi\hbar}{N\Omega} \sum_n |\langle n|\hat{j}_x|0\rangle|^2 \frac{\delta(\hbar|\omega| - E_n + E_0)}{E_n - E_0}, \qquad (D3)$$

where $|n\rangle$ is a many-body state with the energy E_n. By inserting Eq. (D2) in one of the two matrix elements of $\hat{j}_x$, one obtains

$$\frac{2}{\pi} \int_0^\infty \sigma(\omega) d\omega = \frac{e^2}{N\Omega\hbar^2} \langle 0|[[H,\hat{R}_x],\hat{R}_x]|0\rangle. \qquad (D4)$$

Performing the commutators, we find

$$\sum_\alpha [[H,\hat{R}_\alpha],\hat{R}_\alpha] = \sum_{\nu\mu\sigma} d_{\nu\mu}^2 t_{\mu\nu} \psi_{\nu\sigma}^\dagger \psi_{\mu\sigma}, \qquad (D5)$$

where $d_{\nu\mu}$ is the distance between the sites with the orbitals ν and μ and α labels the coordinate. This result is true for the TM model in its semiclassical form, the C_{60} model and

the t–J model. We now assume only nearest-neighbor hopping, replacing $d_{\nu\mu}$ by d. Furthermore, we assume the system to be isotropic, so that all directions α are equivalent. For a three-dimensional system, the commutator on the right-hand side of Eq. (D4) is then one third of the result in Eq. (D5). This gives

$$\frac{2}{\pi}\int_0^\infty \sigma(\omega)d\omega = -\frac{1}{3}\frac{d^2 e^2}{N\Omega\hbar^2}\langle 0|T_K|0\rangle, \qquad (D6)$$

where T_K is the kinetic energy. For a two-dimensional system the factor 3 in the denominator is replaced by a factor 2. This result can also be generalized to a finite temperature. In the case of the TM model, however, the atomic separations cannot be treated as constants, since they vary as the phonons are excited. The coordinates in Eq. (D4) can then not be taken outside the average $\langle\cdots\rangle$. We can, nevertheless, recover an expression such as Eq. (D6) by defining an appropriate average separation $d(T)$.

[1] Z. Fisk and G.W. Webb, Phys. Rev. Lett. **36**, 1084 (1976); Z. Fisk and A.C. Lawson, Solid State Commun. **13**, 277 (1973).

[2] A.F. Ioffe and A.R. Regel, Prog. Semicond. **4**, 237 (1960).

[3] P. B. Allen, in *Superconductivity in d- and f-Band Metals*, edited by H. Suhl and M. B. Maple (Academic, New York, 1980), p. 291.

[4] W. Kohn and J.M. Luttinger, Phys. Rev. **108**, 590 (1957).

[5] B. Chakraborty and P.B. Allen, Phys. Rev. Lett. **42**, 736 (1979).

[6] P.J. Cote and L.V. Meisel, Phys. Rev. Lett. **40**, 1586 (1978).

[7] A. Ron, B. Shapiro, and M. Weger, Philos. Mag. B **54**, 553 (1986).

[8] H. Takagi, B. Batlogg, H.L. Kao, J. Kwo, R.J. Cava, J.J. Krajewski, and W.F. Peck, Jr., Phys. Rev. Lett. **69**, 2975 (1992).

[9] A.F. Hebard, T.T.M. Palstra, R.C. Haddon, and R.M. Fleming, Phys. Rev. B **48**, 9945 (1993).

[10] J.G. Hou, L. Lu, V. Crespi, X.-D. Xiang, A. Zettl, and M.L. Cohen, Solid State Commun. **93**, 973 (1995) have reported a small change in the slope of the resistivity of Rb_3C_{60} for very large T, and interpreted this as the onset of resistivity saturation. The mean free path corresponding to saturation was estimated to be very small, $l \sim 1 \pm 0.5$ Å.

[11] For $La_{1.96}Sr_{0.04}CuO_4$ we have assumed a cylindrical Fermi surface with the height $2\pi/c$, where c is the distance between the CuO_2 planes. The mean free path was assumed to be equal to the Cu-Cu distance in the planes. For C_{60} we assumed the mean free path to be equal to the separation of the C_{60} molecules.

[12] M. Calandra and O. Gunnarsson, Phys. Rev. Lett. **87**, 266601 (2001).

[13] O. Gunnarsson and J.E. Han, Nature (London) **405**, 1027 (2000).

[14] M. Calandra and O. Gunnarsson (unpublished).

[15] R. Blankenbecler, D.J. Scalapino, and R.L. Sugar, Phys. Rev. D **24**, 2278 (1981).

[16] M. Jarrell and J.E. Gubernatis, Phys. Rep. **269**, 134 (1996).

[17] F. Bloch, Z. Phys. **52**, 555 (1928).

[18] G. Grimvall, *The Electron-Phonon Interaction in Metals* (North-Holland, Amsterdam, 1981) pp. 212, 216.

[19] W.E. Pickett, K.M. Ho, and M.L. Cohen, Phys. Rev. B **19**, 1734 (1979).

[20] W. Harrison, *Electronic Structure and the Properties of Solids. The Physics of the Chemical Bond* (Dover, New York, 1980).

[21] O. Jepsen (private communication).

[22] E. L. Wolf, *Principles of Electron Tunnelling Spectroscopy* (Oxford University Press, New York, 1985), p. 268.

[23] O. Gunnarsson, S. Satpathy, O. Jepsen, and O.K. Andersen, Phys. Rev. Lett. **67**, 3002 (1991).

[24] S. Satpathy, V.P. Antropov, O.K. Andersen, O. Jepsen, O. Gunnarsson, and A.I. Liechtenstein, Phys. Rev. B **46**, 1773 (1992).

[25] I.I. Mazin, A.I. Liechtenstein, O. Gunnarsson, O.K. Andersen, V.P. Antropov, and S.E. Burkov, Phys. Rev. Lett. **70**, 4142 (1993).

[26] P.W. Stephens, L. Mihaly, P.L. Lee, R.L. Whetten, S.-M. Huang, R. Kaner, F. Diederichs, and K. Holczer, Nature (London) **351**, 632 (1991).

[27] M. Lannoo, G.A. Baraff, M. Schluter, and D. Tomanek, Phys. Rev. B **44**, 12 106 (1991).

[28] O. Gunnarsson, Phys. Rev. B **51**, 3493 (1995).

[29] J.M. Abraham and B. Deviot, J. Less-Common Met. **29**, 311 (1972).

[30] O. Gunnarsson, Rev. Mod. Phys. **69**, 575 (1997).

[31] L. Pintschovius, Rep. Prog. Phys. **59**, 473 (1996).

[32] P.F. Maldague, Phys. Rev. B **16**, 2437 (1977).

[33] D. A. Papaconstantopoulos, *Hanbook of the Band Structure of Elemental Solids* (Plenum Press, New York, 1986), p. 76.

[34] V.E. Zinov'ev, L.P. Gel'd, G.E. Chuprikov, and K.I. Epifanova, Fiz. Tverd. Tela **14**, 2747 (1972) [Sov. Phys. Solid State **14**, 2747 (1972)].

[35] P.V. Gel'd and V.E. Zinov'ev, High Temp.-High Press. **8**, 523 (1976).

[36] S.Y. Savrasov and D.Y. Savrasov, Phys. Rev. B **54**, 16 487 (1996).

[37] L.F. Mattheiss, L.R. Testardi, and W.W. Yao, Phys. Rev. B **17**, 4640 (1978).

[38] A.J. Bradley and J. Thewlis, Proc. R. Soc. London, Ser. A **115**, 465 (1927).

[39] G.T. Meaden and P. Pelloux-Gervais, Cryogenics **5**, 227 (1965).

[40] H. Wiesmann, M. Gurvitch, H. Lutz, A. Ghosh, B. Schwarz, M. Strongin, P.B. Allen, and J.W. Halley, Phys. Rev. Lett. **38**, 782 (1977).

[41] N. F. Mott, *Metal-insulator Transitions* (Taylor & Francis, London, 1974).

[42] P.A. Lee and T.V. Ramakrishnan, Rev. Mod. Phys. **57**, 287 (1985).

[43] P.D. Antoniou and E.N. Economou, Phys. Rev. B **16**, 3768 (1977).

[44] A.J. Millis, J. Hu, and S. Das Sarma, Phys. Rev. Lett. **82**, 2354 (1999).

[45] In some particular cases (such as the linear chain or the hypercubic lattice) it is possible to perform the so called *checkerboard breakup*, so that Eq. (A2) becomes exact. In these cases it is still possible to perform the standard Quantum Monte Carlo algorithm even in the case of atomic vibrations coupled to the hopping matrix elements.

[46] W. H. Press, *et al.*, *Numerical Recipes, The Art of Scientific Computing*, 2nd ed. (Cambridge University press, Cambridge, 1988).